

# Rock-magnetic and geochemical characteristics of relict Vertisols—signs of past climate and recent pedogenic development

Neli Jordanova and Diana Jordanova

National Institute of Geophysics, Geodesy and Geography, BAS. Acad. G. Bonchev str., bl.3 1113 Sofia, Bulgaria. E-mail: [neli.jordanova@hotmail.com](mailto:neli.jordanova@hotmail.com)

Accepted 2016 February 12. Received 2016 February 11; in original form 2015 May 31

## SUMMARY

Rock-magnetic and geochemical characteristics of three Vertisol profiles with different degree of textural differentiation have been studied. Thermomagnetic analyses, thermal demagnetization of laboratory remanences and acquisition of isothermal remanence curves are applied for identification of iron oxide mineralogy. The main magnetic minerals in Vertisols are ferrihydrite, single-domain magnetite, maghemite and hematite. Variations in magnetic susceptibility, anhysteretic remanent magnetization, isothermal remanent magnetization, as well as different ratios ( $X_{arm}/X$ , ARM/SIRM, S-ratio) along depth are studied. Concentration of magnetic minerals in Vertisols is low, influenced by the intense reductomorphic processes. The lowest magnetic susceptibility is found in the most texturally differentiated soil. However, rock-magnetic data suggest the presence of small, but well defined fraction of single domain-like magnetite with relatively wide grain-size distribution found in those parts of the profiles, which are subjected to most intense and frequent seasonal changes in oxidation-reduction conditions. It is suggested that this fraction is formed as a result of transformations of ferrihydrite under repeated cycles of anaerobic/aerobic conditions. Based on geochemical data, CALMAG weathering index was calculated for the three Vertisols. Using the established relation between CALMAG and mean annual precipitation (MAP), palaeo-MAP was evaluated for the studied profiles. The obtained MAP estimations fall in the range 1000–1200 mm and are much higher compared to contemporary precipitation in the area (MAP in the interval 540–770 mm). This finding confirms the relict character of Vertisols on Bulgarian territory and gives more information about the palaeoclimate during the initial stages of Vertisol formation.

**Key words:** Environmental magnetism; Rock and mineral magnetism.

## 1 INTRODUCTION

Magnetic properties of soils provide very sensitive proxies for the iron oxide formation, transformations, redox dynamics and grain size of the magnetic carriers (Maher 1998; Evans & Heller 2003; Liu *et al.* 2012). The most detailed studies of soil magnetism are carried out on well aerated soils from temperate (Jordanova *et al.* 1997; Evans & Heller 2003; Maher *et al.* 2003) and Mediterranean zones (Liu *et al.* 2010; Torrent *et al.* 2010a,b). These soils exhibit strong magnetic enhancement in their upper horizons as a response to climate conditions (mainly temperature and precipitation) (Maher 1998; Balsam *et al.* 2011). Magnetic studies of soils, subjected to periodic or permanent water logging are restricted to gley soils (Stanjek *et al.* 1994; Dearing *et al.* 1995; Maher 1998; Grimley & Arruda 2007) and paddy soils in China (de Jong 2002; Chen *et al.* 2011; Lu *et al.* 2012; Han & Zhang 2013). Published research on rock- and mineral magnetism of Vertisols is limited and focus on a profile from Mali (Gehring *et al.* 1997; Fisher *et al.* 2007, 2008)

and Texas (USA) (Lindquist *et al.* 2011), developed on alluvium of river terraces. These studies evidence the influence of changing reduction-oxidation conditions on magnetic minerals, leading to reductive dissolution of iron oxides (Cornell & Schwertmann 2003). Fisher *et al.* (2008) show that part of the soil profile, which is most influenced by seasonal water table fluctuations is characterized by lower concentration of magnetic minerals and finer grain sizes as compared to other parts of the solum. The authors suggest that the observed variations in magnetic grain size-related parameters generally reflect the process of reductive dissolution of coarse lithogenic magnetite grains (Grimley & Arruda 2007) under the influence of changing hydrological conditions. No pedogenic fraction of strongly magnetic minerals has been inferred for the tropical Vertisol, based on the obtained negligible frequency-dependent magnetic susceptibility (Gehring *et al.* 1997; Fisher *et al.* 2008).

Since most of the recent Vertisols are developed on Quaternary alluvial sediments (Singh *et al.* 1998; Pal *et al.* 2006), it is supposed that they are young soils. Different studies suggest that minimum

time period for Vertisol development is about 500 yr, though most of the Vertisols in tropical, sub-tropical, as well as in more arid areas, are of Holocene age (Kovda *et al.* 2006; Pal *et al.* 2012). There are also older Vertisols, dated at about 20 000–30 000 yr (Achyuthan *et al.* 2010), and older (Nordt *et al.* 2004). Ancient Vertisol equivalents (paleo-Vertisols) have also been widely identified (Stiles *et al.* 2003 and references therein). A number of studies give evidence that ancient Vertisols effectively preserve morphologic and geochemical characteristics formed in their paleopedogenic settings (Stiles *et al.* 2003). This finding is the basis for the use of Vertisol for palaeoclimate reconstructions (Stiles *et al.* 2001; Nordt & Driese 2010).

Bulgaria is one of the few European countries where Vertisols are found as a dominant soil type in specific regions of their territory (Toth *et al.* 2008). Distribution of Vertisols in Bulgaria is linked to the plain relief of the former Pliocene plateaus and old Quaternary terraces (Koinov *et al.* 1998). During the late Miocene, Alpine tectonics was very active, forcing the uplift of the Carpathians, Dinarides, Balkans, Rhodopes and Caucasus. This led to drying of the Pliocene lakes and expansion of marshland conditions (Koinov *et al.* 1998; Shishkov & Kolev 2014), which favoured development of gley soils, further transformed to Vertisols (Ninov 2002). Subsequently, Vertisols remained unburied on the earth's surface and were subjected to changing climate conditions during the Quaternary. The question about relict signs in Bulgarian Vertisols versus possible transformations, caused by pronounced Quaternary climate fluctuations, is not discussed (Shishkov & Kolev 2014). Moreover, the age of Vertisols found in the different areas in Bulgaria, is uncertain (Shishkov & Kolev 2014) and it is accepted that the age of the soil is determined by the age of the rock-forming parent material. Detailed analytical studies on the palaeoclimate during Vertisols' formation in Bulgaria are practically missing, while abundant data are present on the Miocene climate variations and its parameters (Ivanov *et al.* 2011 and references therein). Thus, our study aims to provide better characterization of magnetic and geochemical signature of pedogenesis in relict Vertisol profiles, which are exposed to changing climate conditions since their initial development. Rock-magnetic and geochemical data for relict Vertisols in the present study allows further elucidation of magnetic pattern of the complex geochemical processes acting in these specific soils, as well as evaluation of palaeoprecipitation during their formation, which would give more information about their age. Comparison between the properties of recent Vertisols (Gehring *et al.* 1997; Fisher *et al.* 2007, 2008), and the investigated relict Vertisols from Bulgaria, would provide a basis for elucidation of several questions: (i) does magnetic signature of relict Vertisols, subjected to seasonal changing redox conditions, match the published data on recent tropical Vertisols?; (ii) what is the reason for possible divergence in the magnetic signatures in these soils? (iii) how the severe climate changes since the supposed initial formation of Vertisols (Pliocene) influence the magnetic signature and properties of these specific soils.

## 2 MATERIAL AND METHODS

### 2.1 Sampling sites

Three profiles of Vertisols were sampled in South Bulgaria. Profile 'VR' (N 42°29'00.9"; E 27°20'37.0") is Epicalcic Mollic Vertisol, located near the town of Burgas. Profile 'JAS' (N 42.283°; E 25.655°) is Mollic Vertisol, sampled near Jastrebovo village (Stara Zagora district). Profile 'SM' (N 41°56'06.3"; E 25°01'14.4") is

Stagnic Endogleyic Vertisol, sampled near Topolovo village (Plovdiv district). The classification is according to World Reference Base for Soil Resources (WRB 2006). Parent material for the profiles VR and JAS is Pliocene carbonate-rich clay. The third profile (SM) is developed on alluvial-delluvial deposits. Short description of the profiles is given in Appendix A.

### 2.2 Sampling and methods

Sampling was done in open pits, having been dug with dimensions about 2 × 1 m and depth about 150 cm. Loose soil material of about 100 g weight was sampled each 2 cm along depth of the profiles using non-metal spatula. Material was stored in plastic bags and then transported to the laboratory. It was air-dried, lightly crushed and sieved through 2 mm sieve. This material was used for magnetic measurements, described below.

Magnetic susceptibility is measured on MFK-1A Kappa bridge (Agico Ltd., Czech Rep.) with sensitivity ( $2 \times 10^{-8}$  SI). Mass-specific magnetic susceptibility ( $\chi$ ) is calculated by normalization to sample's weight. Magnetic susceptibility at liquid nitrogen temperature (77 K) was obtained by immersing the soil samples in liquid nitrogen for 1 hour and then measuring the samples on KLY-2 Kappabridge at room temperature. Since measurement time takes about 1 min., we suggest that the real sample's temperature is not too much deviating from 77 K, to which the low-temperature measurement was ascribed. Laboratory remanent magnetizations were measured on cubic samples, prepared by mixing 2 g of soil material with gypsum and a small amount of water and putting the mixture in plastic cubic forms. Blank gypsum sample was prepared as well and its remanent signal subtracted from those of the samples with soil material. Anhyseretic remanent magnetization (ARM) was induced by Minispin AF demagnetizer (Molspin Ltd., UK) equipped with ARM attachment, applying AF field with maximum amplitude 100 mT and a steady field of 0.1 mT. Isothermal remanent magnetizations (IRM) are imparted by ASC pulse magnetizer (ASC Scientific, USA) with maximum field of 5 T. Step-wise acquisition of IRM in 26 steps up to 5 T is carried out for selected samples from the three Vertisols. The obtained IRM acquisition curves are processed with IRM-CLG1.0 software (Kruiver *et al.* 2001) for evaluation of coercivity components and distributions. Remanent magnetizations (ARM, IRM) were measured on JR6A spinner magnetometer (Agico Ltd., Czech Rep.) with sensitivity  $2 \times 10^{-6}$  A m<sup>-1</sup>. Thermomagnetic analysis of magnetic susceptibility for determination of Curie temperatures of magnetic minerals was carried out in CS-23 furnace attached to KLY-2 susceptibility bridge (Agico, Czech Rep.) on heating from room temperature to 700 °C in air and cooling back, using heating rate of 8 °C min<sup>-1</sup>. Hysteresis measurements were performed in Laboratory for Natural Magnetism (ETH Zurich) using Vibrating sample magnetometer Micromag 3900 (Princeton Measurements Corporation, USA) with maximum applied field of 1 T. Hysteresis loops were corrected for paramagnetic contribution by subtracting the linear part of the loop higher than 700 mT (paramagnetic slope correction). Hysteresis parameters saturation magnetization (Ms), saturation remanence (Mrs) and coercive force (Bc) were calculated. Paramagnetic susceptibility ( $\chi_{\text{hf}}$ ) is calculated from the paramagnetic slope correction. Back-field remanent curves were also measured and the coercivity of remanence (Bcr) determined. Step-wise thermal demagnetizations of laboratory remanences (ARM and IRM) were done in a shielded oven MMTD20 (Magnetic Measurements Ltd., UK) with residual field less than 10 nT. Nodules extracted from depth 70–80 cm of the profile SM and

two levels from profile JAS (147 and 153 cm) were gently crushed and samples for acquisition of IRM were prepared.

Clay, silt and sand fractions (clay  $d < 2 \mu\text{m}$ ; silt  $2 \mu\text{m} < d < 50 \mu\text{m}$  and sand  $d > 50 \mu\text{m}$ ) were determined through wet sedimentation, and results presented as percent values. Organic matter (typically less than 3 per cent) was first removed with 30 per cent  $\text{H}_2\text{O}_2$  and subsequent dispersion with sodium hexametaphosphate applied. Soil pH was measured with a Hanna 213 pH-meter with resolution  $\pm 0.01$  pH (Sigma Aldrich Co., USA) in water using 1:5 soil– $\text{H}_2\text{O}$  proportion. Before measurements, the instrument was calibrated by two-point calibration in buffers pH = 4.01 and pH = 7.01.

Chemical composition of selected samples from each profile was determined by X-ray Fluorescence analysis through energy-dispersive XRF spectrometer Spectro-X-Lab 2000. Acid-oxalate extraction, applying 4 h shaking in dark (McKeague & Day 1966); dithionite-citrate extraction (DCB extraction; Mehra & Jackson 1960) were performed in the Laboratory of Environmental Chemistry at ETH–Zurich. Extracted amounts of Fe, Al and Mn (oxalate extractable—Fe<sub>o</sub>, Al<sub>o</sub>, Mn<sub>o</sub> and dithionite-extractable iron—Fe<sub>d</sub>) were measured by ICP-OES Varian Vista-MPX. For quality checks, blanks were measured in each set of samples. For all extractions two replicas were done from each sample and the values reported per sample are an average of two replicas, deviating typically between 5–10 per cent.

Iron-manganese concretions are characteristic features in Vertisols and are frequently used for palaeoclimate estimations (Stiles *et al.* 2001), based on their Fe-content. Several concretions were picked up from selected depths of the profile ‘SM’ for examination with scanning electron microscope. They were fixed in epoxy resin and polished cross-sections prepared. SEM observations combined with EDX analyses were performed on JEOL JSM6390 scanning electron microscope. EDS analyses in selected points as well as the so-called ‘integral spectrum’ (obtained from EDS scanning the whole cross-section surface of the concretion) are done.

### 3 RESULTS

#### 3.1 Texture classes and geochemistry

Results from the grain size analysis for selected levels from the three Vertisol profiles are summarized in Table 1. Silt fraction dominates the texture in all profiles, comprising between 50–80 per cent of the total. Sand fraction makes up only few percent of the total, although in profiles JAS and SM its content increases in C-horizons up to 8–14 per cent (Table 1). Clay fraction has the biggest share in Calcic Vertisol (VR) with maximum of 49 per cent, while in other two profiles it is still lower. The most differentiated variations in clay content are pertinent to profile SM (Stagnic Vertisol), where maximum clay content is obtained in Ag and Btg horizon. Most of the studies of Vertisols report very high clay content, dominating the texture (Soil Survey Staff 2003; Pal *et al.* 2012), while Bulgarian Vertisols are characterized by relatively lower clay content (Koinov *et al.* 1998). Similar peculiarity is reported for Serbian Vertisols (Jelić *et al.* 2011), for which the mean clay content varies between 33.5–54.4 per cent. Soil reaction (pH) is neutral—to slightly alkaline in the upper humic horizons (Fig. 1) and increases to pH = 8.7 in profile VR, pH = 8.3 in profile JAS and pH = 9.1 in profile SM in the C-horizons. Though quite high, the obtained pH values in the carbonate-rich C-horizons of the profiles are in a good agreement with the published values for Vertisols, sampled in near locations (pH in C horizons between 8.0 and 8.2; Koinov *et al.* 1998) with

**Table 1.** Grain size analysis for selected samples from the three Vertisol profiles.

Sample (depth, cm)	Sand > 50 $\mu\text{m}$ (%)	Silt 50–2 $\mu\text{m}$ (%)	Clay < 2 $\mu\text{m}$ (%)
Profile VR			
4	5.54	60.12	34.34
10	2.36	55.8	41.84
22	3.42	50.54	46.04
30	2.72	48.14	49.14
38	2.74	49.98	47.28
46	3.74	54.98	41.28
56	4.52	58.2	37.28
62	6.16	53.68	40.16
Profile JAS			
3	3.33	68.45	28.22
9	3.6	70.00	26.4
12	2.83	66.07	31.1
42	2.6	58.00	39.4
66	4.02	64.02	31.96
102	3.22	62.62	34.16
132	2.62	70.36	27.02
144	1.22	67.76	31.02
156	4.78	82.2	13.02
174	5.84	81.92	12.24
186	5.43	74.00	20.57
204	7.36	83.22	9.42
Profile SM			
2	6.32	84.56	9.12
10	5.81	83.72	10.46
26	1.94	64.08	33.98
42	5.86	55.76	38.38
62	2.86	63.17	33.97
70	4.61	69.79	25.6
82	8.78	75.78	15.44

the biggest deviation in profile SM. The pH changes are most pronounced in profile SM (Stagnic Vertisol). For this profile pH in the upper horizons (A1 and A2) is the lowest (pH = 6 and below), as well, while for VR and JAS pH is higher than 7.5 in A1 and A2 horizons. The obtained high pH values in C-horizons generally agree with data available about Vertisols in Serbia (Jelić *et al.* 2011—pH varying between 5.8 and 8.1) and Greece (Moustakis 2012—pH in C-horizons between 8.0 and 8.3).

Element concentrations of major and some trace elements for selected depths from the three profiles are summarized in Appendix B. In all three soil profiles Si does not vary significantly in depth, which is a common feature of Vertisols (Schaeztl & Anderson 2009; Shishkov & Kolev 2014). Iron (Fe) and aluminium (Al) show synchronous variations along depth in all three profiles, suggesting their involvement in same oxyhydroxide forms, as shown for many soil types (Cornell & Schwertmann 2003). However, the relative content of Fe in the profiles is different—it is the highest in VR (40–50  $\text{g kg}^{-1}$ ), lower in JAS (35–40  $\text{g kg}^{-1}$ ) and minimum in SM (20–30  $\text{g kg}^{-1}$ ).

Results from oxalate- and dithionite iron extraction for selected samples from the three Vertisol profiles are shown in Table 2 and suggest that Bulgarian Vertisols are characterized by relatively high  $\text{Fe}_o/\text{Fe}_d$  values, as observed for other Vertisols (Fisher *et al.* 2008; Moustakis 2012). Inter-comparison among the profiles confirms an enhancement of the ratio  $\text{Fe}_o/\text{Fe}_d$  with increasing degree of profile textural differentiation from Epicalcic Mollic Vertisol (profile VR) through Mollic Vertisol (JAS) to Endogleyc Vertisol (SM),

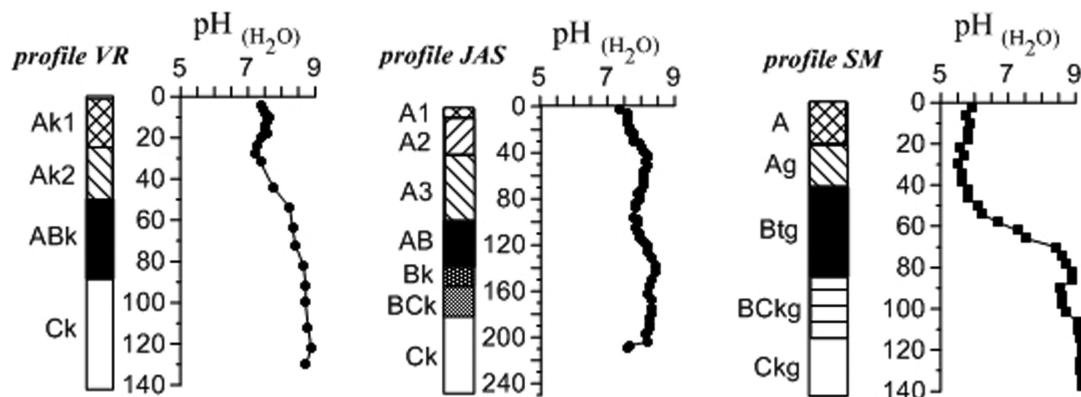


Figure 1. Depth variations of soil pH for Vertisol profiles.

Table 2. Chemical extraction data for Vertisol profiles. Oxalate-extractable Al (Al<sub>o</sub>), Fe (Fe<sub>o</sub>), Mn (Mn<sub>o</sub>); dithionite-extractable iron (Fe<sub>d</sub>), total iron content (Fe total) and the ratios Fe<sub>o</sub>/Fe<sub>d</sub>, Fe<sub>d</sub>/Fe<sub>total</sub>.

Sample No.	Al <sub>o</sub> (g kg <sup>-1</sup> )	Fe <sub>o</sub> (g kg <sup>-1</sup> )	Mn <sub>o</sub> (g kg <sup>-1</sup> )	Fe <sub>d</sub> (g kg <sup>-1</sup> )	Fe total (g kg <sup>-1</sup> )	Fe <sub>o</sub> /Fe <sub>d</sub>	Fe <sub>d</sub> /Fe <sub>total</sub>
Profile VR							
VR2	1.504	1.464	0.233	10.425	45.6	0.140	0.229
VR50	2.127	1.976	0.210	9.175	52.6	0.176	0.213
VR118	0.818	0.679	0.024	11.225	55.4	0.029	0.421
Profile JAS							
JAS3	1.705	1.716	0.558	5.535	35.6	0.310	0.155
JAS12	1.994	2.049	0.604	5.935	38.1	0.345	0.156
JAS66	2.718	2.393	0.533	6.88	39.7	0.348	0.173
JAS144	1.632	0.734	0.532	36.9	36.9		
JAS156	1.540	0.830	0.474	5.34	36.3	0.155	0.147
JAS186	0.897	0.326	0.350	2.57	31.3	0.127	0.082
Profile SM							
SM2	0.738	2.030	0.614	3.85	17.7	0.527	0.218
SM10	0.857	2.485	0.784	3.92	19.2	0.634	0.204
SM26	2.075	1.157	0.368	1.825	36.5	0.634	0.05
SM62	1.224	0.743	1.075	1.735	35.9	0.428	0.048
SM134	0.378	0.00	0.048	2.58	19.3	0.00	0.134

where Fe<sub>o</sub>/Fe<sub>d</sub> reaches a value of 0.6. This association addresses progressively higher Fe amount, involved in reductive dissolution taking place during seasonal water logging and related precipitation of amorphous Fe-phases. On the other hand, the ratio Fe<sub>d</sub>/Fe<sub>total</sub> (dithionite-extractable Fe to the total Fe) is widely used as an indication for the degree of soil maturity (Cornell & Schwertmann 2003). In the three studied Vertisols Fe<sub>d</sub>/Fe<sub>total</sub> is higher in soil horizons and decreases in C-horizons. The obtained data are in agreement with previously published results for Mollic Vertisol from Bulgaria (Jockova & Boyadjiev 1993), reporting Fe<sub>d</sub>/Fe<sub>total</sub> between 0.26–0.33 in soil horizons. For SM profile the ratios Fe<sub>o</sub>/Fe<sub>total</sub> and Fe<sub>d</sub>/Fe<sub>total</sub> exhibit well expressed depth variations with clear maximum in the upper 20 cm (Table 2). In Mollic Vertisols (profiles VR and JAS) the amount of extracted Fe<sub>o</sub> and Al<sub>o</sub> is very similar, both residing probably in amorphous Fe-hydroxides.

### 3.2 Magnetic parameters

#### 3.2.1 Magnetic minerals identification

Thermomagnetic analysis of magnetic susceptibility is used for identification of magnetic minerals in selected samples from Vertisol profiles and representative results are shown in Fig. 2. All samples are characterized by intensive phase transformations after heating to 700 °C, leading to very high increase in magnetic

susceptibility on cooling. Heating runs for materials from the uppermost 2–3 cm of the profiles (Figs 2a, d and g) exhibit similar behaviour with a small peak at ~300 °C, followed by a decrease and further stronger increase with maximum peak at 500 °C. Final fast drop at 580 °C marks the Curie temperature of magnetite. Similar magnetic susceptibility behaviour is often observed for well aerated soils, enhanced with fine pedogenic maghemite particles (Maher 1986; Maher & Taylor 1988; Maher & Thompson 1995). The identified magnetite phase could be an initially present magnetite fraction, as well as a secondary transformation product resulting from hematite's reduction during its heating in the presence of organic matter. Thermomagnetic analyses for soil samples from deeper parts of the Vertisols with pronounced seasonal anaerobic conditions show contrasting behaviour. It is not straightforward to interpret unambiguously phase transformations occurring in the range (200–300 °C), since several minerals show changes in this interval—ferrihydrite, as well as lepidocrocite (Gehring & Hofmeister 1994; Mitov *et al.* 2002; Hanesch *et al.* 2006). The observed transformation behaviour gives clues for the presence of ferrihydrite, taking into account the observations of Hanesch *et al.* (2006). Both samples from the C-horizons of profiles JAS and SM exhibit an initial very fast decrease in  $\chi$  up to 200 °C and magnetite's T<sub>c</sub> (Figs 2f and i), which suggest the presence of magnetite as lithogenic mineral. A small fraction is left after magnetite's Curie temperature, indicating hematite occurrence.

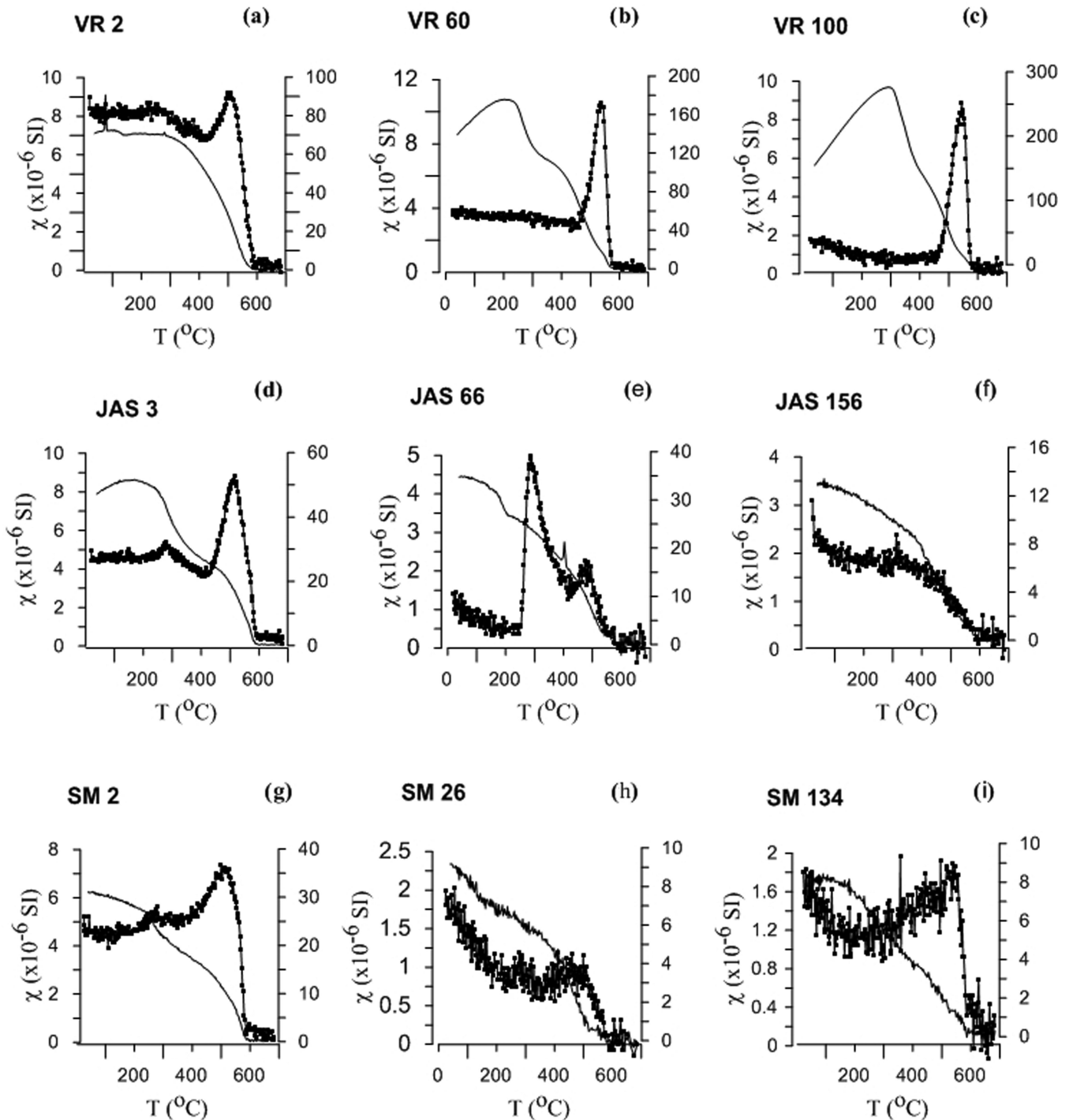


**Figure 2.** High-temperature behaviour of magnetic susceptibility during heating to 700 °C (thick curve) and cooling back to room temperature (thin line, secondary y-axis) for selected samples from profile VR (a–c); JAS (d–f) and SM (g–i). Heating in air.

Characterization of the stable, remanence-carrying ferromagnetic fraction in Vertisols is extended by step-wise thermal demagnetization of isothermal remanent magnetization (IRM; Fig. 3). In all samples the component, saturated in (0–1) Tesla field is much stronger than the high-coercivity component (1–2) Tesla. It is clear, however, that in profile VR the relative contribution of high-coercivity component to the total remanent magnetization is systematically larger, as compared with the samples from profile

SM (Fig. 3). The high-coercivity component in VR is demagnetized in the temperature range (200–250 °C) (Figs 3a and b). Two unblocking temperatures are visible in the soft IRM component (0–1 T)—at 300 °C and 580 °C for all samples, which could be related to maghemite and magnetite, respectively. Step-wise thermal demagnetization of anhysteretic remanence (ARM) for two samples from the illuvial horizon of the profile SM (Fig. 4) demonstrates the presence of stable fraction single-domain like magnetite, which is

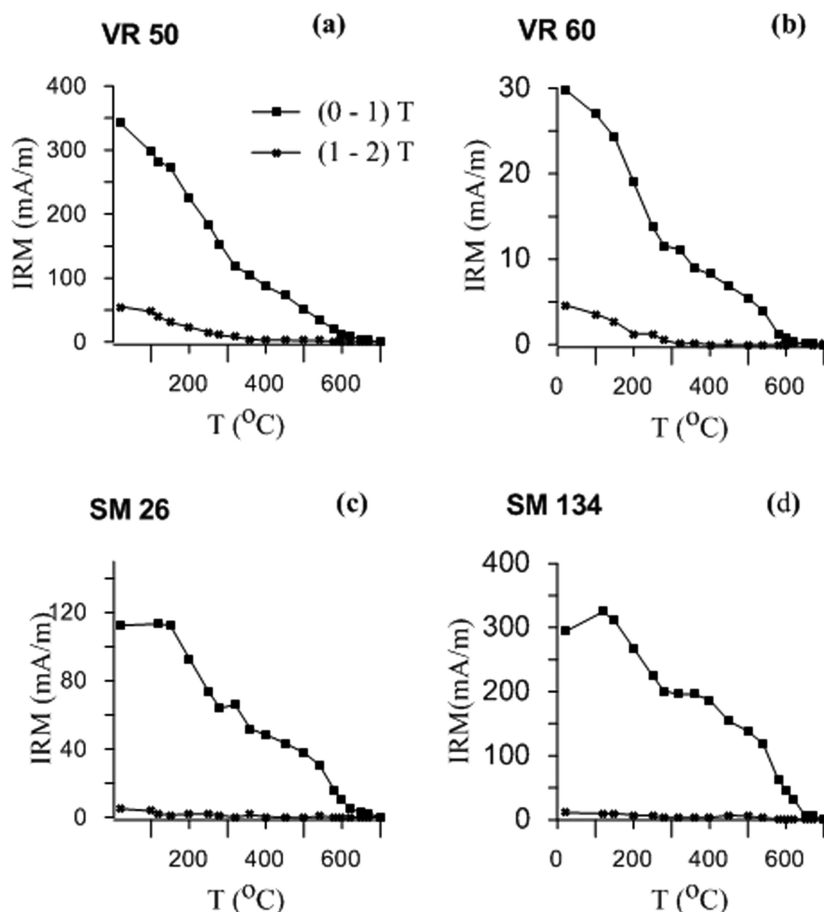


Figure 3. Step-wise thermal demagnetization of two-component IRM (0–1 T) and (1–2 T) for selected samples from profiles VR and JAS.

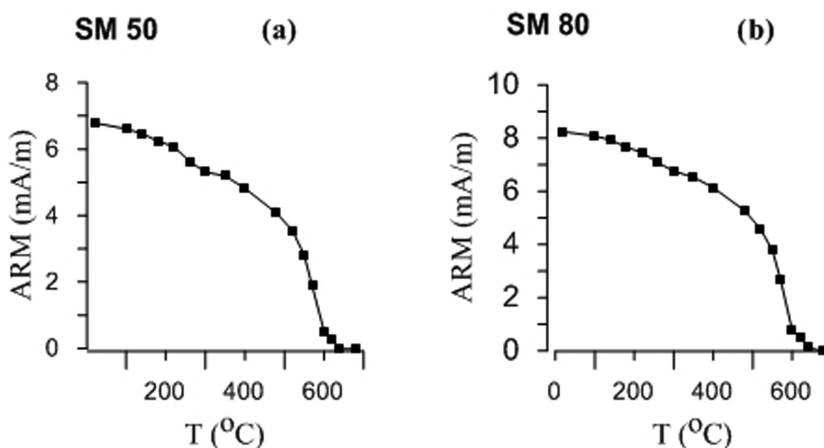


Figure 4. Step-wise thermal demagnetization of ARM for two samples from profile SM.

expressed through convex curve and sharp unblocking at 580 °C. A small fraction of maghemite is unblocked at higher temperatures of about 640 °C.

### 3.2.2 Step-wise acquisition of IRM and analysis of coercivity components

Step-wise acquisition curves of IRM are shown in Fig. 5. Samples from profiles of Epicalcic Mollic Vertisol (VR) and Mollic Vertisol (JAS) do not reach saturation up to 5 T, suggesting the presence

of high coercivity minerals, while samples from the Endogleyic Vertisol (SM) saturate in fields of about 600 mT (Figs 5a–c). Summarized results from the coercivity analysis, carried out according to Kruiver *et al.* (2001) approach for the three profiles are presented in Table 3. Two coercivity components best approximate the acquisition curves for samples from VR and JAS. Low-coercivity component in all samples has stronger magnetization than the high-coercivity one. The field at which half of the SIRM is reached—the parameter  $B_{1/2}$ —is relatively uniform along depth of the profiles (Table 3). The dispersion parameter DP varies in the range 0.35–0.42, implying wider coercivity distribution, which could reflect

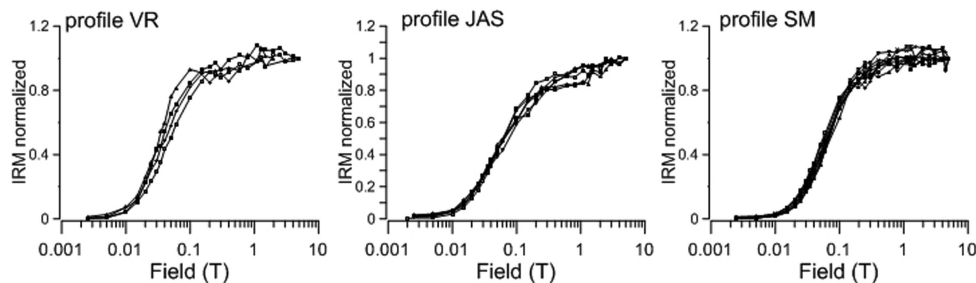


Figure 5. IRM acquisition curves for samples from the three Vertisol profiles.

Table 3. Summary parameters from IRM-CLG1.0 (Kruiver *et al.* 2001) software application for Vertisols. Intensity, median acquisition field ( $B_{1/2}$ ) and dispersion parameter (DP) for each coercivity component identified is presented. Analyses of IRM-acquisition curves for concretions from profiles JAS and SM are also shown (samples denoted 'Concr.').

Sample No.	IRM component 1			IRM component 2		
	Intensity ( $\text{mAm}^2 \text{kg}^{-1}$ )	$B_{1/2}$ (mT)	DP	Intensity ( $\text{mAm}^2 \text{kg}^{-1}$ )	$B_{1/2}$ (mT)	DP
Epicalcic Mollic Vertisol VR						
VR 2	6.58	45.7	0.42	0.41	891.3	0.24
VR 20	2.10	36.3	0.39	0.32	794.3	0.25
VR50	1.29	29.9	0.29	0.29	891.3	0.45
VR116	2.04	34.7	0.35	0.38	794.3	0.37
Mollic Vertisol JAS						
JAS6	1.88	44.7	0.32	0.57	631.0	0.50
JAS51	0.38	42.7	0.40	0.17	3162.3	0.62
JAS108	0.36	45.7	0.42	0.15	5623.4	0.61
Concr. JAS 147	2.39	30.2	0.41	–	–	–
Concr. JAS 153	1.67	31.6	0.44	0.13	631.0	0.50
JAS150	0.80	42.7	0.42	0.22	467.7	0.37
JAS183	0.56	43.7	0.40	0.14	562.3	0.36
JAS 210	0.43	50.1	0.46	0.15	575.4	0.53
Stagnic Endogleyic Vertisol SM						
SM2	4.50	51.3	0.36	–	–	–
SM6	2.71	60.3	0.36	–	–	–
SM10	2.60	60.3	0.38	–	–	–
SM26	0.90	66.1	0.47	–	–	–
SM42	1.32	60.3	0.35	0.62	1000.0	0.33
SM62	1.33	67.6	0.38	–	–	–
SM66	1.05	66.1	0.47	–	–	–
Concr. SM 70–80	2.01	58.9	0.36	0.25	1584.9	0.23
SM134	2.35	72.4	0.39	–	–	–
SM138	1.65	61.7	0.35	–	–	–

natural wide grain size spectra of the corresponding phases. High-coercivity component in profile VR shows  $B_{1/2}$  between (790 and 890) mT, while in JAS it is softer in upper levels (JAS6) and at the bottom of profile (150 cm and below). Coercivities of the second IRM component, characteristic for VR and JAS are more typical for hematite, which saturates in fields between 500 mT and 2 T, depending on the grain size and shape of the particles, foreign substitutions in the crystal lattice and formation pathway (Dunlop & Ozdemir 1997; de Boer & Dekkers 1998; Peters & Dekkers 2003; Jiang *et al.* 2012; Hu *et al.* 2013). Samples from the middle parts of profile JAS (51 and 108 cm) contain a component with very high coercivity (Table 3), which could be ascribed to goethite.

### 3.2.3 Depth variations of magnetic parameters

Variations in magnetic parameters and ratios, related to concentration and grain size of the magnetic fraction along Vertisol pro-

files are shown in Figs 6–8. Variations in low-field magnetic susceptibility  $\chi_{lf}$  (Figs 6a, 7a and 8a) along the three profiles are not linked to the genetic soil horizons, but are characterized by more or less smooth decrease in depth. Epicalcic Mollic Vertisol (VR profile) is distinguished by the highest values of  $\chi_{lf}$  (reaching  $\sim 75 \times 10^{-8} \text{ m}^3 \text{ kg}^{-1}$ ), while in the other two profiles (JAS and SM)  $\chi_{lf}$  is rather low (typically  $10\text{--}20 \times 10^{-8} \text{ m}^3 \text{ kg}^{-1}$ ). Such values suggest very low concentration of strongly magnetic minerals and the prevailing role of paramagnetic fraction in  $\chi_{lf}$  (e.g. Dearing 1999). This is confirmed by the high-field magnetic susceptibility ( $\chi_{hf}$ ). In all profiles  $\chi_{hf}$  has minimum in the uppermost humic horizons and shows increasing contribution downwards (Figs 6b, 7b and 8b), well corresponding to the obtained variations in silt and clay fraction (Table 1). Calculated correlation coefficients between  $\chi_{hf}$  and clay/silt ratio for the three profiles are respectively  $R^2 = 0.64$  (profile VR);  $R^2 = 0.63$  (profile JAS) and  $R^2 = 0.84$  (profile SM). It is noticeable that the Endogleyic Vertisol (SM profile) exhibits the most

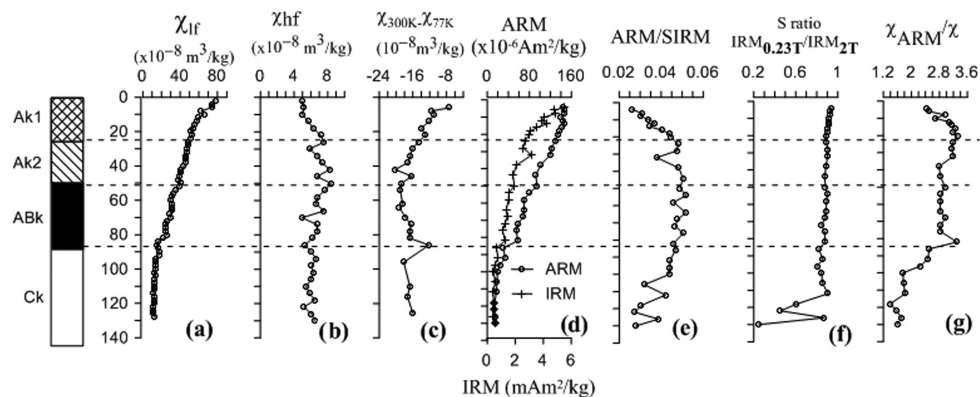


**Figure 6.** Depth variations of (a) low-field magnetic susceptibility ( $\chi_{lf}$ ); (b) high-field magnetic susceptibility ( $\chi_{hf}$ ); (c)  $\chi_{TD} = \chi_{300K} - \chi_{77K}$ ; (d) anhysteretic remanence (ARM) and isothermal remanence (IRM); (e) ratio ARM/SIRM; (f) S-ratio, defined as  $IRM_{0.23T}/IRM_{2T}$ ; (g) ratio  $\chi_{ARM}/\chi$  for Epicalcic Mollic Vertisol (profile VR).

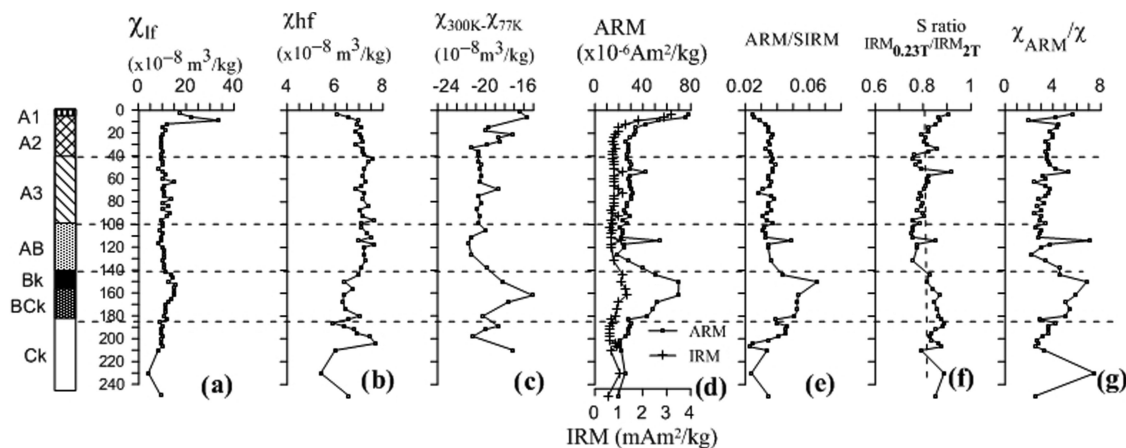


**Figure 7.** Depth variations of (a) low-field magnetic susceptibility ( $\chi_{lf}$ ); (b) high-field magnetic susceptibility ( $\chi_{hf}$ ); (c)  $\chi_{TD} = \chi_{300K} - \chi_{77K}$ ; (d) anhysteretic remanence (ARM) and isothermal remanence (IRM); (e) ratio ARM/SIRM; (f) S-ratio defined as  $IRM_{0.23T}/IRM_{2T}$ ; (g) ratio  $\chi_{ARM}/\chi$  for Mollic Vertisol (profile JAS).

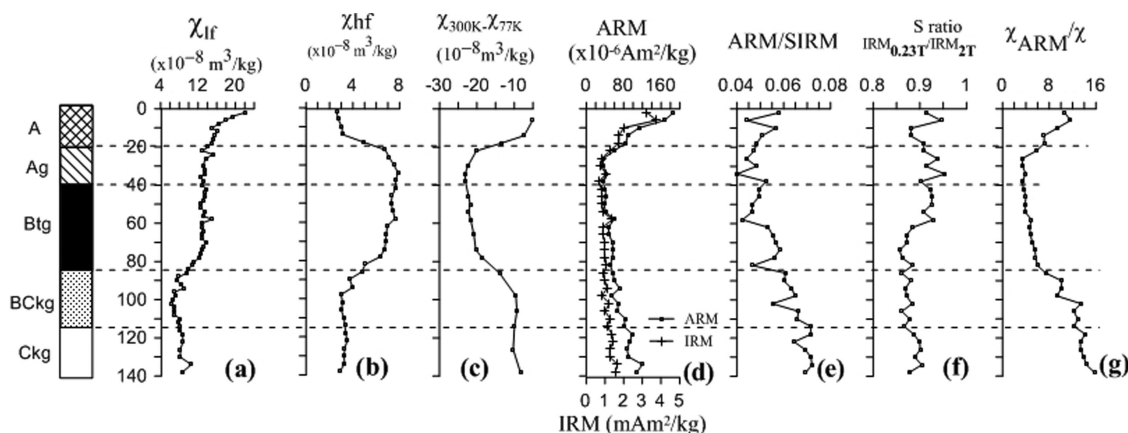


**Figure 8.** Depth variations of (a) low-field magnetic susceptibility ( $\chi_{lf}$ ); (b) high-field magnetic susceptibility ( $\chi_{hf}$ ); (c)  $\chi_{TD} = \chi_{300K} - \chi_{77K}$ ; (d) anhysteretic remanence (ARM) and isothermal remanence (IRM); (e) ratio ARM/SIRM; (f) S-ratio defined as  $IRM_{0.23T}/IRM_{2T}$ ; (g) ratio  $\chi_{ARM}/\chi$  for Endogleyic Vertisol (profile SM).

differentiated variations in all magnetic characteristics, in line with its strong textural contrast (Table 1). Confirmation about the dominant role of paramagnetic fraction in determination of  $\chi_{hf}$  comes also from the variations in the parameter  $\chi_{TD}$ —the difference between low-field magnetic susceptibility, measured at room temperature (300 K) and at liquid nitrogen temperature (77 K) ( $\chi_{TD} = \chi_{300K}$

$-\chi_{77K}$ ) (Figs 6c, 7c and 8c). Wang & Løvlie (2008), who define this parameter, show that it depends on the prevailing content among paramagnetic minerals, superparamagnetic (SP) and single-domain (SD) magnetite particles in the sample. SP particles would be in an SD state at 77 K and thus  $\chi_{TD}$  will be positive. In case of prevailing paramagnetic fraction,  $\chi_{77K} > \chi_{300K}$  because of increase in

susceptibility of paramagnets according to the Curie law (O'Reilly 1984). Magnetite particles, passing through the Verwey transition at 120 K will also exhibit decrease in magnetic susceptibility at 77 K. Therefore, the obtained negative  $\chi_{TD}$  for the Vertisols is related to the presence of significant amount of paramagnetic (clay) minerals. For the three Vertisol profiles  $\chi_{TD}$  has minimum values in A1 and Btg horizons (Figs 6c, 7c and 8c). Magnetic remanences (ARM and IRM) trace variations in remanence-carrying fractions along the three profiles. In Epicalcic Mollic Vertisol (VR profile) IRM shows general similarity with  $\chi_{IF}$  (Fig. 6d), while ARM trend is characterized by a more convex shape in Ak1 and Ak2 horizons, compared to IRM variations. This behaviour suggests an enhancement of middle portions of Ak1 down to Ak2 with stable SD grains, with concentration decreasing in depth. Grain-size related parameter  $\chi_{ARM}/\chi$  suggests that the most stable (true SD) fraction of pedogenic magnetite is found at the boundary between Ak1 and Ak2 horizons, where  $\chi_{ARM}/\chi$  shows maximum (Fig. 6g). Well expressed enhancement of Ak1, Ak2 and ABk horizons with SD magnetite fraction is also distinguished by the higher ARM/SIRM in these soil horizons. The S-ratio is high (between 0.8 and 0.9) along the soil horizons and only in the deepest levels of the C horizon shows significant contribution of high-coercivity minerals (Fig. 6f). Variations of IRM along the profile of Mollic Vertisol JAS reveal similar features to those along the profile VR. Anhyseretic remanence however, is strongly enriched in Bk and Bck horizons, evidencing enrichment with stable SD grains. ARM/SIRM and  $\chi_{ARM}/\chi$  variations with maxima in Bk and Bck horizons (Figs 7e and g) indicate the presence of the finest SD grains there. Spike-like SD enrichment is also observed at about 110 cm depth (Figs 7d–g). The S-ratio for JAS profile is oscillating around 0.8 along depth (Fig. 7f). Endogleyic Vertisol (profile SM) is enhanced with remanence carrying ferromagnetic fraction in the upper A horizon (Fig. 8d), where both IRM and ARM have clear maxima, while clay-rich Ag and Btg horizons are relatively depleted. In the C-horizon ARM and IRM again show gradual increase, related most probably to the presence of lithogenic remanence carrying grains. Based on this behaviour, ARM/SIRM and  $\chi_{ARM}/\chi$  have increased values also in the bottom part of the profile (Figs 8e and g). Thus, single-domain magnetic fraction is restricted to the upper A horizon and Bckg–Ckg horizons. The S-ratio (Fig. 8f) is higher in the upper half of the profile and has lower values in deeper horizons. Comparison among the three Vertisol profiles shows that the distribution of stable SD grain size fraction becomes increasingly more differentiated with maxima shifted to uppermost A horizon and lower parts of the profile (Bckg and Ckg horizons) with increasing degree of textural differentiation (Epicalcic–Mollic–Endogleyic).

### 3.2.4 Hysteresis parameters

Hysteresis parameters Ms and Mrs show depth variations, very similar to these of  $\chi$  and IRM2T, respectively, and they are shown in Appendix C. Coercivity parameters Bc and Bcr vary little in depth. There are however, systematic differences in coercivity values among the three Vertisol profiles—the highest Bc and Bcr are observed for the profile SM, while the lowest ones are pertinent to the profile VR (Appendix C). Grain size dependent ratios Mrs/Ms and Bcr/Bc are plotted on a Day plot (Day *et al.* 1977; Dunlop 2002a,b) for the three Vertisols and shown in Fig. 9. All data group in the PSD area, but it is evident that profile VR is most shifted towards coarser PSD grain sizes, while JAS and SM show higher Mrs/Ms and lower Bcr/Bc (Fig. 9). Considering the theoretical mixing curves

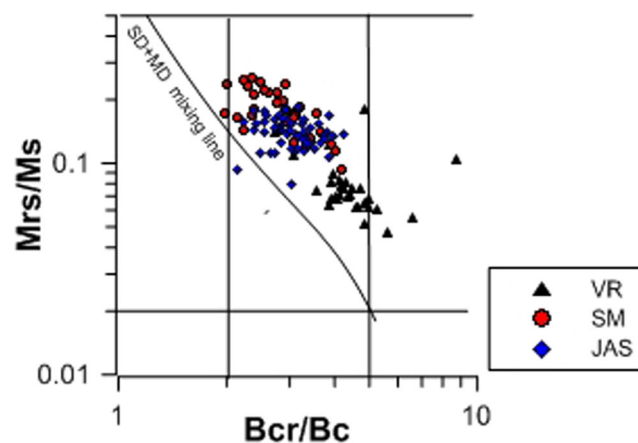


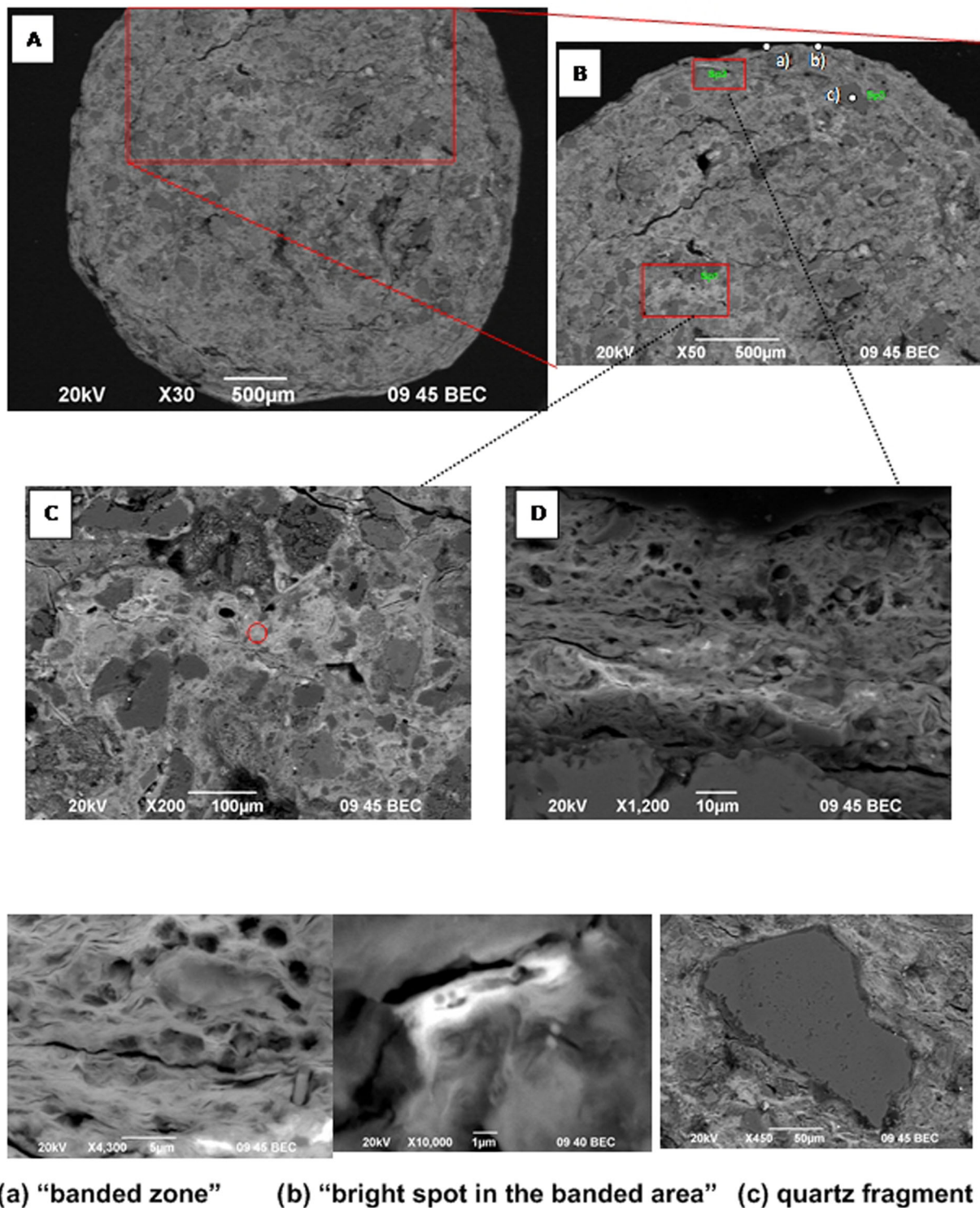
Figure 9. Day plot (Day *et al.* 1977; 2002a,b) for samples from different depth levels from the three Vertisols.

for different grain size fractions (Dunlop 2002a,b), it could be noticed that data for the three Vertisols plot close to (SD+MD) mixing curve. The biggest contribution of the SD fraction is seen therefore for the profile of Endogleyic Vertisol (SM), in agreement also with the coercivity analysis of IRM acquisition curves (Table 3).

### 3.3 Scanning electron microscopy (SEM) and magnetic measurements of soil nodules

As shown in the soil profile's description, abundant concretions/nodules were found in the Vertisols, but they are especially numerous in the Endogleyic Vertisol SM. SEM observations were done on a cross-section of a coarse nodule (~4 mm diameter), extracted from the soil material from depth of (70–80) cm (Btg soil horizon). Several images in back-scattered electrons mode are shown in Fig. 10 and EDS data are summarized in Table 4. SEM images of the nodule (Fig. 10) reveal non-differentiated structure inside, with abundant soil particles, incorporated in the matrix. Cracks with no preferential orientation are also observed (Figs 10A and B). Specific feature of the nodule is its well-developed outer shell with concentric structure, pores and fibrous features (Figs 10A and D). Enhanced content of Fe, Mn and Si is seen from the EDS analyses in different parts of the concretion (Table 4).

In order to study the magnetic properties of concretions, IRM-acquisition is carried out on powdered material from different depths of the profiles JAS and SM. Results from coercivity analysis of IRM acquisition curves for nodules are shown in Table 3 (denoted by 'concr.') together with the results for the bulk soil samples. Coercivity analysis of IRM acquisition curves for nodules from profile JAS reveals the presence of two components—low coercivity with  $B_{1/2} = 30$  and 31.6 mT (Table 3) and high coercivity with  $B_{1/2} = 630$  mT, detected only in the deeper sample. Compared with the coercivity of the soft component for soil samples from JAS profile (Table 3), it is clear that the nodules contain magnetically softer ferrimagnetic mineral, while the identified hard component is consistent with the coercivity of the hematite's phase in soil. However, the intensity of the soft IRM component in nodules is significantly higher (~3-fold) than in soil (Table 3), demonstrating an enhanced concentration of strongly magnetic Fe-oxides there. Similarly, nodules from profile SM show lower coercivity and higher intensity of the soft component compared to soil material (Table 3).



(a) “banded zone” (b) “bright spot in the banded area” (c) quartz fragment

**Figure 10.** SEM images in back-scattered electrons mode of soil nodule from Endogleyic Vertisol (SM), depth 70–80 cm. Images C and D are enlarged areas, where spectra Sp1 and Sp2 are taken. Locations of higher-resolution images (a–c) are indicated on image B.

## 4 DISCUSSION

### 4.1 Magnetic susceptibility in Vertisol profiles

Studies of polygenetic soils always face difficulties to separate relict from recent features, because different stages in soil development are only partially preserved or some of them are practically miss-

ing (Fedoroff *et al.* 2010). Substantial climate changes since the Pliocene (Abrantes *et al.* 2012), inevitably influence Vertisols development during their exposition at the Earth’s surface, including also their magnetic characteristics. Since Vertisols developed on flat geomorphological forms, erosion did not play significant role during their pedogenesis. In agreement with other studies of magnetism of soils, conditioned by permanent or seasonal water-logging (Dearing

**Table 4.** EDS spectra in selected spots (denoted on Fig. 10) of nodule from profile SM (depth 70–80 cm) and ‘integral spectrum’ obtained for the whole diametric surface. Elements shown in weight per cent.

Element	Integral spectrum (whole nodule) (weight %)	Zone Sp1 (weight %)	Zone Sp2 (weight %)	‘Banded’ zone above Sp2 (weight %)	Bright spot in the banded area above Sp2 (weight %)
O	52.36	45.3	46.11	44.06	35.61
Na	1.85	–	–	–	–
Mg	0.00	0.92	0.38	0.77	–
Al	6.07	3.70	4.22	6.35	2.44
Si	19.30	6.23	10.22	15.67	6.28
K	2.19	1.43	0.81	2.02	2.50
Ca	0.89	2.44	1.86	1.94	–
Mn	7.42	33.96	9.51	13.75	9.77
Fe	9.91	1.85	17.18	14.53	10.09
Ba	–	4.16	–	0.90	–
Ce	–	–	9.70	–	33.31
Total	100	100	100	100	100

*et al.* 1995; Maher 1998; de Jong 2002; Grimley & Arruda 2007; Lu *et al.* 2012), Bulgarian Vertisols are characterized by very low magnetic susceptibility. On the other hand, since they are considered in the Bulgarian soil science as relict soils, comparison with properties of typical contemporary Vertisol will help elucidate the magnetic signal due to Vertisol genesis from those, linked to more recent processes. Variations of magnetic susceptibility along the profile from Mali (Gehring *et al.* 1997) resemble those of Bulgarian Vertisols (Figs 6a, 7a and 8a) with maximum at the surface ( $\chi_{lf} = 86 \times 10^{-8} \text{ m}^3 \text{ kg}^{-1}$ ), followed by gradual decrease up to  $\chi_{lf} = 17 \times 10^{-8} \text{ m}^3 \text{ kg}^{-1}$  in Ag-horizon, laying immediately above the summer level of the water table (Gehring *et al.* 1997). Therefore, maximum value of  $\chi_{lf}$  of the tropical Vertisol is close to the maximum value of  $\chi_{lf}$  for the Vertisol VR (Fig. 6a), while the Mollic Vertisol JAS and Endogleyic Vertisol SM show significantly lower magnetic susceptibilities in their profiles (Figs 7a and 8a). On the other hand, the Vertisol from Texas (Lindquist *et al.* 2011) shows quite higher values of magnetic susceptibility ( $200 \times 10^{-8} \text{ m}^3 \text{ kg}^{-1}$ ), in spite of the very similar trend in the depth variations. The most probable reason is an enhanced concentration of lithogenic magnetic particles in the alluvial deposits, on which the Texas Vertisol developed.

#### 4.2 Magnetic minerals in Vertisols and their origin

The main magnetic mineral, identified in the contemporary Vertisol from Mali (Gehring *et al.* 1997; Fisher *et al.* 2008) is oxidized magnetite. In the Vertisol from Texas (Lindquist *et al.* 2011) the major magnetic minerals found are magnetite, maghemite and goethite/hematite in deeper horizons. Thermomagnetic curves of samples from the uppermost levels in Bulgarian Vertisols (Figs 2a, d and g) closely resemble the ones obtained for upper horizons of Chernozem-type soils from Bulgaria (Jordanova *et al.* 1997; Jordanova *et al.* 2010), Russia (Maher *et al.* 2003), China (Liu *et al.* 2005) and Luvisols from Spain (Liu *et al.* 2010). Thus, it can be assumed that the observed high-temperature curves for surface levels of the Vertisols show the presence of pedogenic maghemite, formed under favourable locally well aerated conditions. Very similar thermomagnetic curve is reported for the uppermost Ap horizon in the tropical soil from Mali (Fisher *et al.* 2008). Magnetic results obtained from the IRM acquisition curves for deeper soil horizons suggest that the main magnetic minerals are low-coercivity magnetite-like phase, as well as hematite (in profiles VR and JAS) and goethite in few depth intervals in profile

JAS (Table 3). It is also notable, that our results, as well as the published studies on contemporary Vertisols (Gehring *et al.* 1997; Fisher *et al.* 2008; Lindquist *et al.* 2011) all detect the presence of magnetite of relatively fine grain size in the soil profiles. Magnetic characteristics, which are proxies for the grain size of magnetite (ARM/SIRM,  $\chi_{ARM}/\chi$ ) for all the three profiles in our study clearly show systematic increase in concentration of the SD magnetite from the surface towards the deeper A horizons in profiles VR (Ak2), JAS (A2) and SM (Ag) (Figs 6–8). These sub-surface horizons are seasonally anaerobic, with perched water table and intense weathering of lithogenic minerals. The presence of stable SD magnetite fraction also in BCK- and BCKg horizons of the profiles JAS and SM (Figs 7 and 8) suggests that in the deeper soil horizons, affected mostly by groundwater table fluctuations, stable fraction of magnetite is also present. Fisher *et al.* (2008) in their study of subtropical Vertisol also observe decreasing grain size of magnetite-like fraction with increasing soil depth. They conclude, that the observed decrease downward from the surface level is most probably due to the effect of maghemitization of lithogenic iron oxide particles during reductive dissolution of iron oxides (Grimley & Arruda 2007) in the profile’s part, which is most influenced by water table fluctuations. The authors suggest that in the upper Ap horizon of their Vertisol magnetic grains are predominantly in MD state. This hypothesis is based on the premises that the lithogenic fraction, consisting of coarse magnetite particles is responsible for the observed magnetic properties of the Vertisol. Direct re-translation of similar processes to explain the magnetic behaviour in the studied three profiles faces several questions, which cannot be answered applying the mechanism proposed by Fisher *et al.* (2008). These are the following: (1) well expressed enhancement with stable (SD-PSD) magnetite/maghemite fraction of the uppermost A horizon of all three profiles, as suggested by ARM remanence and ratios variations (Figs 6–8); and (2) missing regular increase of coercivity parameters (as obtained for the tropical Vertisol profile) in profiles’ levels most influenced by redoximorphic changes (Appendix C). In addition, thermomagnetic behaviour of magnetic susceptibility for the soils’ depths, influenced by intense redox changes (Figs 2b, c, e and h) suggest the presence of thermally unstable iron oxyhydroxides, most probably ferrihydrite and goethite. Therefore, explanation of the observed magnetic properties of Bulgarian Vertisols required seeking other geochemical processes active in seasonally changing redox conditions in soils. The most widespread iron oxyhydroxide

in soil terrestrial environments is ferrihydrite (Schwertmann 1988; Cornell & Schwertmann 2003), which is also the most reactive and bioavailable FeIII mineral for respiration of iron reducing bacteria. In spite that we do not have direct identification data of ferrihydrite in the studied profiles, the transformation behaviour of magnetic susceptibility of soil samples (Fig. 2) strongly supports its presence in the middle part of the solum. This supposition is supported also by the obtained relatively high values of Feo/Fed ratio (Table 2), since ferrihydrite is among the Fe oxides, which contribute the most to the oxalate-extractable Fe (Feo) (Cornell & Schwertmann 2003). As it is seen from Table 2, Feo/Fed is higher in the upper horizons of the profiles SM and JAS, while in VR it is lower. Numerous studies show that the transformation products of ferrihydrite reductive dissolution depend on the Fe<sup>2+</sup> concentration (Hansel *et al.* 2005, 2011; Piepenbrock *et al.* 2011). Lower Fe<sup>2+</sup> concentrations promote goethite and lepidocrocite mineralization, while high supply rates promote magnetite nucleation and growth (Hansel *et al.* 2011). Thus, possible mechanism for the formation of stable SD-like magnetite phase in Vertisols is its nucleation and growth as a result of ferrihydrite reductive dissolution in the presence of Fe<sup>2+</sup> in the (seasonal) fluid flow through the soil profile. Adsorption and substitution of Al and Si impedes ferrihydrite transformation to more crystalline phases—magnetite, goethite, lepidocrocite (Ekstrom *et al.* 2010; Hansel *et al.* 2011). As it was shown for the three Vertisols studied, total Si and Al content varies among the three profiles, being the highest in profile SM, followed by JAS and VR (Appendix B). Therefore, it could be supposed that increased Si and Al content in SM impede the transformation of ferrihydrite and thus smaller amount of magnetite could be nucleated. In line with this hypothesis is the obtained lowest magnetic susceptibility and remanent magnetization values in the profile SM (Fig. 8). The SD-like fraction of magnetite produced would not dominate the magnetic concentration-related parameters (like magnetic susceptibility and IRM) but it is well expressed in ARM, as is demonstrated by the experimental data.

#### 4.3 Iron (oxy)hydroxides in a Vertisol—signs of relict climate or recent pedogenic development?

Recent climate conditions, influencing Vertisol's pedogenesis are characterized by significantly lower precipitation and lower temperature, as compared to the ancient climate during the Pliocene. Vertisols are subjected to seasonal multiple reduction-oxidation cycles, which could be considered as an analogue of advective flow, causing reductive dissolution of ferrihydrite, according to Hansel *et al.* (2003). As demonstrated in a model study (Hansel *et al.* 2011) ferrihydrite does not transform when high Al-content is present in the soil solution and goethite precipitates under lower Fe<sup>2+</sup> concentration. According to the IRM acquisition curves and transformation behaviour of magnetic susceptibility during heating (Fig. 2, Table 3), ferrihydrite and goethite are probably present in deeper levels of the three Vertisols, which is in agreement with the above considerations. Crystalline remanence-carrying Fe-containing phases detected through the magnetic measurements (Figs 2 and 3, Table 3) are magnetite(maghemite) and hematite in profiles VR and JAS (Fig. 5, Table 3), while in profile SM only magnetite was detected (with exception of one sample—Table 3). In Endogleyic Vertisol SM, however, because of the strong textural differentiation (Table 1), anaerobic conditions probably prevail during most of the year and magnetite is preserved non-oxidized. In addition, Thompson *et al.* (2006) demonstrate that as a result of periodic

oscillations in reductive conditions, crystallinity of the secondary mineral phases formed (goethite and hematite) increases with increasing number of cycles at the expense of decrease in amount of nano-crystalline minerals. Taking into account the above results, it could be supposed that the Endogleyic Stagnic Vertisol (profile SM) underwent the most frequent reduction-oxidation cycles among the three profiles studied, and the resulting grain size of the secondary magnetite is the finest, as evidenced by the magnetic results (Table 3).

Single domain-like magnetite fraction, detected through the magnetic proxies (Figs 4, 6–8) is concentrated in those parts of Vertisol profiles, which are most influenced by water level (perched water table or ground water table) fluctuations—in the upper horizons (A1-A2) and in deeper levels—in ABk/BCk (Figs 6–8). The obtained evidence for uniform grain size distribution of the ARM-carrying fraction (as deduced from the convex shape of thermal ARM demagnetization curves, Fig. 4) supports the hypothesis for nucleation of SD/small PSD magnetite as a result of abiotic ferrihydrite transformation, which produces narrow well defined magnetite grains (Miot *et al.* 2014), but with larger grain-size compared to magnetite, produced by magnetotactic bacteria (Hansel *et al.* 2003).

Since ferrihydrite is thermodynamically unstable mineral (Cornell & Schwertmann 2003), it is not likely that it has been preserved in Vertisols since their initial formation. This leads to the conclusion, that the detected ARM-carrying fraction (most likely fine grained magnetite), closely linked to the profiles' parts, which are exposed to most frequent redox changes, is formed in Vertisols under more recent climate. This could also explain the differences in magnetic properties of our relict Vertisols and the tropical soil from Mali (Gehring *et al.* 1997; Fisher *et al.* 2008). Obtained evidence about maghemitization of lithogenic magnetite grains in the recent Vertisol (Fisher *et al.* 2008), explaining its magnetic signature, may have also been active in our Vertisols during their initial development. A clue to such supposition is the obtained higher ARM and its ratios in the bottom part of profile SM (Fig. 8).

#### 4.4 Nodules in Vertisols and their palaeoenvironmental significance

Morphology of iron-manganese nodules from the studied Vertisols (Fig. 10) is similar to the one described for nodules from Vertisols of Cambodia (Mitsuchi 1976), for which however preferential radial direction of cracks in the core is observed as well. Analogous soil nodules are reported for Ultisols from Taiwan, used for rice cropping (Jien *et al.* 2010). Elemental composition, as deduced from the 'integral spectrum' (Table 4) indicates enhanced concentration of Si, Mn and Fe. High Silica content most probably is due to the incorporated soil particles, which are enriched in Si. Comparison between the EDS spectra measured in Sp1 spot and the integral spectrum (Table 4) demonstrates big heterogeneity in Fe and Mn distribution in nodule's core. Taking into account that Sp1 area is positioned close to the centre of the nodule, it could be supposed that this inner part is relatively enriched in Mn (34 per cent) as compared to the rim. Similar distribution is obtained by Jien *et al.* (2010) for Taiwan Vertisols. EDS spectra, taken close to the rim (around Sp2 area—Figs 10B and D) show enhanced Fe content at the expense of Mn (Table 4).

Studies on mineralogy of soil concretions and nodules from soils, characterized by periodic change of oxidative and reductive conditions show that the dominant Fe-oxides/hydroxides are goethite and ferrihydrite (Zhang & Karathanasis 1997; Liu *et al.* 2002; Cornu

*et al.* 2009; Laveuf *et al.* 2012), but Mitsuchi (1976) also proves the presence of maghemite and hematite in nodules from Vertisols. Furthermore, Singh & Gilkes (1996) studied Fe-containing concretions from different Australian soils, subjected to seasonal water-logging and prove the presence of goethite, hematite and maghemite. Schwertmann & Taylor (1989) suggest that hematite is found in palaeoconcretions as a result of post-pedogenic dehydration of goethite. Magnetic data (IRM coercivity analysis) for nodules from Bulgarian Vertisols show the presence of maghemite and hematite, rather than goethite. Taking into account also that nodules have sharp external boundaries within the soil (field observations), it could be supposed that they have been formed during the initial development stage of the Vertisols during the Pliocene, rather than in the Holocene.

In the studies of Vertisols and their potential use as palaeoclimate indicator, Stiles *et al.* (2001) showed that the total Fe content of nodules from Vertisols is correlated with the mean annual precipitation (MAP) by a well-defined regression line. The obtained 'integral' EDS spectra of the nodule from profile SM (Table 4) shows relatively high Fe content—about 10 per cent. In spite that the analysis is not representative, since the data relates to only one nodule, comparison with the obtained regression between Fe(total) and MAP (Stiles *et al.* 2001) gives an approximate MAP value of about 1000 mm. The obtained value is significantly higher than the present-day MAP value in the sampled location (MAP = 768 mm; Appendix A) and supports relict character of the nodules in Bulgarian Vertisols.

#### 4.5 Palaeoweathering index CALMAG, estimated for relict Vertisols from Bulgaria

Weathering indexes are frequently used in rainfall estimates in different environments (Sheldon *et al.* 2002). The first universal weathering index for rainfall estimates CIA-K, defined by Sheldon *et al.* (2002), makes use of the fact that relative to  $\text{Al}_2\text{O}_3$  content, the basic oxides CaO, MgO,  $\text{Na}_2\text{O}$  and  $\text{K}_2\text{O}$  become depleted with increasing rainfall (e.g. weathering). The weathering index is defined as  $\text{CIA-K} = \text{Al}_2\text{O}_3 / (\text{Al}_2\text{O}_3 + \text{CaO} + \text{Na}_2\text{O}) \times 100$ , where CIA-K is the chemical index of alteration minus potassium. Potassium is not considered in the index because of the potential effects of illitization. This index is widely used for different soil types, but Nordt & Driese (2010) detailed its applicability especially to Vertisols. They show that for this specific soil variety it is more appropriate to track the fluxes of Ca and Mg, supplied from calcium carbonate, detrital clay, and exchangeable  $\text{Ca}^{2+}$  and  $\text{Mg}^{2+}$ . Thus, Nordt & Driese (2010) suggest the use of the modified weathering index, called CALMAG, which is expressed as:  $\text{CALMAG} = \text{Al}_2\text{O}_3 / (\text{Al}_2\text{O}_3 + \text{CaO} + \text{MgO}) \times 100$ . Compared to CIA-K, MgO is substituted for  $\text{Na}_2\text{O}$ , aimed at reducing the influence of differential inheritance and weathering of sodium-bearing primary minerals. The authors found a better linear regression between the CALMAG index and the mean annual precipitation (MAP) for a Vertisol climo-sequence, spanning wide MAP variations, compared to the use of CIA-K index. The regression is defined by the relation:  $\text{MAP} = 22.69 \times \text{CALMAG} - 435.8$ . Later, Adams *et al.* (2011) showed also that CALMAG proxy provides a more robust MAP estimate for Vertisols, compared to CIA-K index. In addition, the authors prove that paleorainfall estimates determined from paleofloras, confirm that the CALMAG method is reliable for reconstructing MAP from ancient Vertisols.

The weathering index CALMAG was calculated for our three Vertisol profiles, taking the results from the XRF analyses. The

three chemical elements were transformed to oxide forms. For each profile CALMAG is obtained as an average of the individual estimations along depth, excluding the uppermost 20 cm, as recommended by Nordt & Driese (2010), in order to avoid possible interference of external material deposited on the surface. The following CALMAG values were obtained for the three profiles: (1) profile VR: CALMAG = 66.8; (2) profile JAS: CALMAG = 68.0; (3) profile SM: CALMAG = 68.8. Using the linear regression between MAP and CALMAG (Nordt & Driese 2010), the corresponding MAP for the three Vertisols, is as follows:  $1079 \pm 58$  mm (VR profile, determination from 2 depth levels);  $1108.0 \pm 79$  mm (JAS profile, determination from 10 depth levels) and  $1125 \pm 68$  mm (SM profile, determination from 7 depth levels). In contrast, contemporary MAP values for the studied locations are much lower: for VR MAP = 543 mm, for JAS MAP = 576 mm and for SM MAP = 768 mm (Koinov *et al.* 1998).

According to the proposed hypotheses (Ninov 2002), Vertisol formation in Bulgaria began in the late Pliocene, when most of the Pliocene lakes dry out as a result of tectonic uplift. Therefore, Vertisols genesis and evolution in Bulgaria are considered tectonically and hydrologically predetermined, and not so much influenced by changing climate factors (Ninov 2002; Nachev & Dimitrov 2015). Taking into account these assumptions, we could suppose that the obtained estimates for MAP through CALMAG indexes reflect the palaeoclimatic conditions during the initial vertic stage of the soil development in a climate, characterized by significantly higher precipitation and temperatures in the late Pliocene. A number of palaeoflora studies from the region (Ivanov *et al.* 2007, 2011) indicate significant climate change at the end of the late Miocene from warm sub-tropical conditions with MAP in the interval 800–1300 mm to drier climate during Pliocene and Quaternary. Studies on Early Pliocene plant assemblages from Bulgaria (Palamarev *et al.* 1999; Kovar-Eder *et al.* 2006) show that beech-deciduous oak-hornbeam forests predominated and climatic proxies inferred MAP in the interval (800–1200 mm). The MAP estimate obtained from the three Vertisol profiles, as well as the rough estimate from the Fe-Mn nodule, corresponds to the upper limit of MAP palaeoflora estimates for the Pliocene in Bulgaria.

## 5 CONCLUSIONS

Magnetic properties of relict Vertisols from Bulgaria reveal complex iron (oxy)hydroxide mineralogy, produced during pedogenic development in different climatic regimes since the Pliocene. Magnetic depletion due to intense iron oxide dissolution in anaerobic conditions results in weak magnetization and magnetic susceptibility along the soil profiles. The main magnetic minerals identified in the three Vertisol profiles, are magnetite, maghemite and hematite. Soil horizons, experiencing seasonal reduction-oxidation changes due to specific water regime of Vertisols, are characterized by the presence of a small, but well defined fraction of single-domain like magnetite. It is suggested that this fraction represents a transformation product of reductive dissolution of ferrihydrite. SEM observations coupled with EDX analyses show that soil nodules are enhanced with iron and manganese and display specific internal structure. Magnetic properties of nodules from Vertisols demonstrate strong enhancement with maghemite, as compared to the soil material. Based on the obtained geochemical data for selected samples from different depth intervals of the three Vertisols, the weathering index CALMAG (Nordt & Driese 2010) is calculated. Based on this weathering index, a proxy estimation of MAP for the studied profiles shows

values in the interval 1000–1200 mm and thus gives information about palaeoclimate conditions during the initial formation of these soils.

## ACKNOWLEDGEMENTS

This work is partially supported by research projects DFNI K02/13 ‘Fire in the past, recorded in archaeological remains and soils—implications for archaeology and soil science from a rock-magnetic perspective’ funded by Bulgarian National Science Fund and project SCOPES 2005–2008 ‘Environmental applications of soil magnetism for sustainable land use’ project No IB7320-110723/1. Constructive comments made by M. Dekkers and an anonymous reviewer helped a lot for improvement of the manuscript.

## REFERENCES

- Abrantes, F. *et al.*, 2012. Paleoclimate variability in the Mediterranean, in *The Climate of the Mediterranean Region*, pp. 1–86, ed. Lionello, P., Elsevier.
- Achyuthan, H., Flora, O., Braidia, M., Shankar, N. & Stenni, B., 2010. Radiocarbon ages of pedogenic carbonate nodules from Coimbatore region, Tamil Nadu, *J. Geol. Soc. India*, **75**, 791–798.
- Adams, J., Kraus, M. & Wing, S., 2011. Evaluating the use of weathering indices for determining mean annual precipitation in the ancient stratigraphic record, *Palaeogeogr. Palaeoclimatol. Palaeoecol.*, **309**, 358–366.
- Balsam, W.L., Ellwood, B.B., Ji, J., Williams, E.R., Long, X. & El Hassani, A., 2011. Magnetic susceptibility as a proxy for rainfall: worldwide data from tropical and temperate climate, *Quat. Sci. Rev.*, **30**(19–20), 2732–2744.
- Cornell, R. & Schwertmann, U., 2003. *The Iron Oxides: Structure, Properties, Reactions, Occurrence and Uses*, Wiley-VCH.
- Chen, L.-M., Zhang, G.-L. & Efland, W.R., 2011. Soil characteristic response times and pedogenic thresholds during the 1000-year evolution of a paddy soil chronosequence, *Soil Sci. Soc. Am. J.*, **75**(5), 1807–1820.
- Cornu, S., Cattle, J., Samouëlian, A., Laveuf, C., Guilherme, L. & Alberic, P., 2009. Impact of redox cycles on manganese, iron, cobalt, and lead in nodules, *Soil Sci. Soc. Am. J.*, **73**, 1231–1241.
- Day, R., Fuller, M. & Schmidt, V.A., 1977. Hysteresis properties of titanomagnetites—grain size and compositional dependence, *Phys. Earth Planet. Inter.*, **13**, 260–267.
- Dearing, J., 1999. Magnetic susceptibility, in *Environmental Magnetism: A Practical Guide*, pp. 35–62, eds. Walden, J., Oldfield, F. & Smith, J., Quaternary Research Association, Technical Guide No. 6.
- Dearing, J., Lees, J. & White, C., 1995. Mineral magnetic properties of acid gleyed soils under oak and Corsican Pine, *Geoderma*, **68**, 309–319.
- De Boer, C. & Dekkers, M., 1998. Thermomagnetic behaviour of haematite and goethite as a function of grain size in various non-saturating magnetic fields, *Geophys. J. Int.*, **133**, 541–552.
- de Jong, E., 2002. Magnetic susceptibility of Gleysolic and Chernozemic soils in Saskatchewan, *Can. J. Soil Sci.*, **82**, 191–199.
- Dunlop, D., 2002a. Theory and application of the Day plot (Mrs/Ms versus Hcr/Hc). 1. Theoretical curves and tests using titanomagnetite data, *J. geophys. Res.*, **107**(B3), 2056, doi:10.1029/2001JB000486.
- Dunlop, D., 2002b. Theory and application of the Day plot (Mrs/Ms versus Hcr/Hc). 2. Application to data for rocks, sediments and soils, *J. geophys. Res.*, **107**(B3), 2057, doi:10.1029/2001JB000487.
- Dunlop, D. & Ozdemir, O., 1997. *Rock Magnetism: Fundamentals and Frontiers*, Cambridge Studies in Magnetism Series, Cambridge Univ. Press.
- Ekstrom, E., Learman, D., Madden, A. & Hansel, C., 2010. Contrasting effects of Al substitution on microbial reduction of Fe(III) (hydr)oxides, *Geochim. Cosmochim. Acta*, **74**, 7086–7099.
- Evans, M. & Heller, F., 2003. *Environmental Magnetism: Principles and Applications of Enviromagnetics*, Academic Press.
- Fedoroff, N., Courty, M.-A. & Guo, Zh., 2010. Palaeosols and relict soils, in *Interpretation of Micromorphological Features of Soils and Regoliths*, pp. 623–662, eds. Stoops, G., Marcelino, V. & Mees, F., Elsevier.
- Fischer, H., Luster, J. & Gehring, A.U., 2007. EPR evidence for maghemitization of magnetite in a tropical soil, *Geophys. J. Int.*, **169**(3), 909–916.
- Fisher, H., Luster, J. & Gehring, A., 2008. Magnetite weathering in a Vertisol with seasonal redox-dynamics, *Geoderma*, **143**, 41–48.
- Gehring, A. & Hofmeister, A., 1994. The transformation of lepidocrocite during heating: a magnetic and spectroscopic study, *Clays Clay Miner.*, **42**(4), 409–415.
- Gehring, A., Guggenberger, G., Zech, W. & Luster, J., 1997. Combined magnetic, spectroscopic, and analytical-chemical approach to infer genetic information for a vertisol, *Soil Sci. Soc. Am. J.*, **61**(1), 78–85.
- Grimley, D. & Arruda, N., 2007. Observations of magnetite dissolution in poorly drained soils, *Soil Sci.*, **172**(12), 968–982.
- Han, G.-Z. & Zhang, G.-L., 2013. Changes in magnetic properties and their pedogenetic implications for paddy soil chronosequences from different parent materials in south China, *Eur. J. Soil Sci.*, **64**(4), 435–444.
- Hansel, C., Benner, S., Netss, J., Dohnalkova, A., Kukkadapu, R. & Fendorf, S., 2003. Second mineralization pathways induced by dissimilatory iron reduction of ferrihydrite under advective flow, *Geochim. Cosmochim. Acta*, **67**(16), 2977–2992.
- Hansel, C., Benner, S. & Fendorf, S., 2005. Competing Fe(II)-induced mineralization pathways of ferrihydrite, *Environ. Sci. Technol.*, **39**, 7147–7153.
- Hansel, C., Learman, D., Lentini, C. & Ekstrom, E., 2011. Effect of adsorbed and substituted Al on Fe(II)-induced mineralization pathways of ferrihydrite, *Geochim. Cosmochim. Acta*, **75**, 4653–4666.
- Hanesch, M., Stanjek, H. & Petersen, N., 2006. Thermomagnetic measurements of soil iron minerals: the role of organic carbon, *Geophys. J. Int.*, **165**, 53–61.
- Hu, P., Liu, Q., Torrent, J., Barron, V. & Jin, Ch., 2013. Characterizing and quantifying iron oxides in Chinese loess/paleosols: implications for pedogenesis, *Earth planet. Sci. Lett.*, **369–370**, 271–283.
- Ivanov, D., Ashraf, A. & Mosbrugger, V., 2007. Late Oligocene and Miocene climate and vegetation in the Eastern Paratethys area (northeast Bulgaria), based on pollen data, *Palaeogeogr. Palaeoclimatol. Palaeoecol.*, **255**, 342–360.
- Ivanov, D., Utescher, T., Mosbrugger, V., Syabryaj, S., Djordjević-Milutinović, D. & Molchanoff, S., 2011. Miocene vegetation and climate dynamics in Eastern and Central Paratethys (Southeastern Europe), *Palaeogeogr. Palaeoclimatol. Palaeoecol.*, **304**, 262–275.
- Jelić, M., Milivojević, J., Trifunović, S., Dalović, I., Milošev, D. & Šeremešić, S., 2011. Distribution and forms of iron in the vertisols of Serbia, *J. Serb. Chem. Soc.*, **76**(5), 781–794.
- Jiang, Zh., Liu, Q., Barrón, V., Torrent, J. & Yu, Y., 2012. Magnetic discrimination between Al-substituted hematites synthesized by hydrothermal and thermal dehydration methods and its geological significance, *J. geophys. Res.*, **117**, B02102, doi:10.1029/2011JB008605.
- Jien, S.H., Hseu, Z.Y., Iizuka, Y., Chen, T.H. & Chiu, C.Y., 2010. Geochemical characterization of placic horizons in subtropical montane forest soils, Northeastern Taiwan, *Eur. J. Soil Sci.*, **61**, 319–332.
- Jockova, M. & Boyadjiev, T., 1993. Forms of the Iron, Aluminum and Manganese compounds in certain soils in Bulgaria, *Forest Sci.*, **2**, 62–71 (in Bulgarian with English abstract).
- Jordanova, D., Petrovsky, E., Jordanova, N., Evlogiev, J. & Butchvarova, V., 1997. Rockmagnetic properties of recent soils from North Eastern Bulgaria, *Geophys. J. Int.*, **128**, 474–488.
- Jordanova, D., Jordanova, N., Petrov, P. & Tsacheva, T., 2010. Soil development of three Chernozem-like profiles from North Bulgaria revealed by magnetic studies, *Catena*, **83**(2–3), 158–169.
- Koynov, V., Kabakchiev, I. & Boneva, K., 1998. *Atlas of Soils in Bulgaria*, Zemizdat.
- Kovar-Eder, J., Kvaček, Z., Martinetto, E. & Roiron, P., 2006. Late Miocene to Early Pliocene vegetation of southern Europe (7–4 Ma) as reflected in the megafossil plant record, *Palaeogeogr. Palaeoclimatol. Palaeoecol.*, **238**, 321–339.
- Kovda, I., Mora, C. & Wilding, L., 2006. Stable isotope compositions of pedogenic carbonates and soil organic matter in a temperate climate Vertisol with gilgai, southern Russia, *Geoderma*, **136**, 423–435.

- Kruiver, P., Dekkers, M. & Heslop, D., 2001. Quantification of magnetic coercivity components by the analysis of acquisition curves of isothermal remanent magnetization, *Earth planet. Sci. Lett.*, **189**, 269–276.
- Laveuf, C., Cornu, S., Guilherme, R.L., Guerin, A. & Juillot, F. 2012. The impact of redox conditions on the rare earth element signature of redoximorphic features in a soil sequence developed from limestone, *Geoderma*, **170**, 25–38.
- Lindquist, A., Feinberg, J. & Waters, M., 2011. Rock magnetic properties of a soil developed on an alluvial deposit at Buttermilk Creek, Texas, USA, *Geochem. Geophys. Geosyst.*, **12**(12), Q12Z36, doi:10.1029/2011GC003848.
- Liu, F., Colombo, C., Adamo, P., He, J. & Violante, A., 2002. Trace elements in manganese-iron nodules from Chinese Alfisol, *Soil Sci. Soc. Am. J.*, **66**, 661–171.
- Liu, Q., Deng, Ch., Yu, Y., Torrent, J., Jackson, M., Banerjee, S. & Zhu, R., 2005. Temperature dependence of magnetic susceptibility in an argon environment: implications for pedogenesis of Chinese loess/palaeosols, *Geophys. J. Int.*, **161**, 102–112.
- Liu, Q., Hu, P., Torrent, J., Barrón, V., Zhao, X., Jiang, Zh. & Su, Y., 2010. Environmental magnetic study of a Xeralf chronosequence in north-western Spain: indications for pedogenesis, *Palaeogeogr. Palaeoclimatol. Palaeoecol.*, **293**, 144–156.
- Liu, Q., Roberts, A., Larrasoaña, J., Banerjee, S., Guyodo, Y., Tauxe, L. & Oldfield, F., 2012. Environmental magnetism: principles and applications, *Rev. Geophys.*, **50**, RG4002, doi:10.1029/2012RG000393.
- Lu, S.-G., Zhu, L. & Yu, J.-Y., 2012. Mineral magnetic properties of Chinese paddy soils and its pedogenic implications, *Catena*, **93**, 9–17.
- Maher, B., 1986. Characterization of soils by mineral magnetic measurements, *Phys. Earth planet. Inter.*, **42**, 76–92.
- Maher, B.A., 1998. Magnetic properties of modern soils and Quaternary loessic paleosols: paleoclimatic implications, *Palaeogeogr. Palaeoclimatol. Palaeoecol.*, **137**, 25–54.
- Maher, B. & Taylor, R., 1988. Formation of ultra fine-grained magnetite in soils, *Nature*, **336**, 368–370.
- Maher, B. & Thompson, R., 1995. Paleorainfall reconstructions from pedogenic magnetic susceptibility variations in the Chinese loess and paleosols, *Quat. Res.*, **44**, 383–391.
- Maher, B., Alekseev, A. & Alekseeva, T., 2003. Magnetic mineralogy of soils across the Russian Steppe: climatic dependence of pedogenic magnetite formation, *Palaeogeogr. Palaeoclimatol. Palaeoecol.*, **201**, 321–341.
- McKeague, J.A. & Day, J.H., 1966. Dithionite and oxalate extractable Fe and Al as aids in differentiating various classes of soils, *Can. J. Soil Sci.*, **46**(1), 13–22.
- Mehra, O. & Jackson, M., 1960. Iron oxide removal from soils and clays by a dithionite-citrate system buffered with sodium bicarbonate, *Clays Clay Miner.*, **7**, 317–327.
- Miot, J., Li, J., Benzerara, K., Sougrati, M., Ona-Nguema, G., Bernard, S., Jumas, J.-C. & Guyot, F., 2014. Formation of single domain magnetite by green rust oxidation promoted by microbial anaerobic nitrate-dependent iron oxidation, *Geochim. Cosmochim. Acta*, **139**, 327–343.
- Mitov, I., Paneva, D. & Kunev, B., 2002. Comparative study of the thermal decomposition of iron oxyhydroxides, *Thermochim. Acta*, **386**, 179–188.
- Mitsuchi, M., 1976. Characteristics and genesis of nodules and concretions occurring in soils of the R. Chinit area, Kompong Thom Province, Cambodia, *Soil Sci. Plant Nutr.*, **22**(4), 409–421.
- Moustakis, N., 2012. A study of Vertisol genesis in North Eastern Greece, *Catena*, **92**, 208–215.
- Nachev, G. & Dimitrov, I., 2015. Relationship between the soil types, topography and the parent rocks in Southeast Bulgaria, *Rev. Bulg. Geol. Soc.*, **76**(1), 51–68.
- Ninov, N., 2002. Soils, in *Geography of Bulgaria*, pp. 277–317, eds, Kopravev, I., Yordanova, M. & Mladenov, Ch., Institute of Geography – Bulg. Acad. Sci., ForCom.
- Nordt, L., Wilding, L., Lynn, W. & Crawford, C., 2004. Vertisol genesis in a humid climate of the coastal plain of Texas, USA, *Geoderma*, **122**, 83–102.
- Nordt, L. & Driese, S., 2010. New weathering index improves paleorainfall estimates from Vertisols, *Geology*, **38**(5), 407–410.
- O'Reilly, W., 1984. *Rock and Mineral Magnetism*, Blakie.
- Pal, D., Bhattacharyya, T., Chandran, P., Ray, S., Srivastava, P., Durge, S. & Bhuse, S., 2006. Significance of soil modifiers (Ca-zeolites and gypsum) in naturally degraded vertisols in the peninsular India in redefining the sodic soils, *Geoderma*, **136**, 210–228.
- Pal, D., Wani, S. & Sahrawat, K., 2012. Vertisols of tropical Indian environments: pedology and edaphology, *Geoderma*, **189–190**, 28–49.
- Palamarev, E., Ivanov, D. & Bozukov, V., 1999. Paläoflorenkomplexe im Zentralbalkanischen Raum und ihre Entwicklungsgeschichte von der Wende Oligozän/Miozän bis ins Villafranchium, *Flora Tertiaria Mediterranea*, **VI 5**, 1–95.
- Peters, C. & Dekkers, M., 2003. Selected room temperature magnetic parameters as a function of mineralogy, concentration and grain size, *Phys. Chem. Earth*, **28**, 659–667.
- Piepenbrock, A., Dippon, U., Porsch, K., Appel, E. & Kappler, A., 2011. Dependence of microbial magnetite formation on humic substance and ferrihydrite concentrations, *Geochim. Cosmochim. Acta*, **75**, 6844–6858.
- Singh, B. & Gilkes, R., 1996. Nature and properties of iron rich glaucoites and mottles from some south-west Australian soils, *Geoderma*, **71**, 95–120.
- Singh, L., Parkash, B. & Singhvi, A., 1998. Evolution of the lower Gangetic Plain landforms and soils in West Bengal, India, *Catena*, **33**, 75–104.
- Schaetzl, R. & Anderson, A., 2009. *Soils: Genesis and Geomorphology*, Cambridge Univ. Press.
- Schwertmann, U., 1988. Occurrence and formation of iron oxides in various pedoenvironments, in *Iron in Soils and Clay Minerals, NATO ASI Series: Series C: Mathematical and Physical Sciences*, Vol. 217, pp. 267–308, eds, Stucki, J., Goodman, B. & Schwertmann, U., Reidel Publ. Company.
- Schwertmann, U. & Taylor, R., 1989. Iron oxides, in *Minerals in Soil Environments*, 2nd edn, pp. 379–438, eds, Dixon, J.B. & Weed, S.B., Soil Science Society of America Book series No. 1.
- Sheldon, N., Retallack, G. & Tanaka, S., 2002. Geochemical climofunctions from North American soils and application to paleosols across the Eocene-Oligocene boundary in Oregon, *J. Geol.*, **110**, 687–696.
- Shishkov, T. & Kolev, N., 2014. *The Soils of Bulgaria, World Soils Book Series*, p. 205, ed. Hartemink, A.E., Springer Science+Business Media.
- Stanjek, H., Fassbinder, J.W.E., Vali, H., Wügele, H. & Graf, W., 1994. Evidence of biogenic greigite (ferromagnetic Fe<sub>3</sub>S<sub>4</sub>) in soil, *Eur. J. Soil Sci.*, **45**, 97–103.
- Stiles, C., Mora, C. & Driese, C., 2001. Pedogenic iron-manganese nodules in Vertisols: a new proxy for paleoprecipitation?, *Geology*, **29**, 943–946.
- Stiles, C., Mora, C. & Driese, S., 2003. Pedogenic processes and domain boundaries in a Vertisol climosequence: evidence from titanium and zirconium distribution and morphology, *Geoderma*, **116**, 279–299.
- Soil Survey Staff, 2003. *Keys to Soil Taxonomy*, 9th edn, United States Dept. Agriculture, Natural Resources Conservation Service.
- Thompson, A., Chadwick, O., Rancourt, D. & Chorover, J., 2006. Iron oxide crystallinity increases during soil redox oscillations, *Geochim. Cosmochim. Acta*, **70**, 1710–1727.
- Torrent, J., Liu, Q. & Barrón, V., 2010a. Magnetic minerals in Calcic Luvisols (Chromic) developed in a warm Mediterranean region of Spain: origin and paleoenvironmental significance, *Geoderma*, **154**, 465–472.
- Torrent, J., Liu, Q.S. & Barrón, V., 2010b. Magnetic susceptibility changes in relation to pedogenesis in a Xeralf chronosequence in northwestern Spain, *Eur. J. Soil Sci.*, **61**, 161–173.
- Toth, G., Montanarella, L., Stolbovoy, V., Mate, F., Bodis, K., Jones, A., Panagos, P. & Van Liedekerke, M., 2008. *Soils of the European Union, JRC Scientific and Technical Reports*, Luxembourg Office for Official Publications of the European Communities.
- Wang, R. & Løvlie, R., 2008. SP-grain production during thermal demagnetization of some Chinese loess/palaeosol, *Geophys. J. Int.*, **172**, 504–512.
- World Reference Base for Soil Resources, 2006. *A Framework for International Classification, Correlation and Communication*, FAO/ISRIC.
- Zhang, M. & Karathanasis, A., 1997. Characterization of iron-manganese concretions in Kentucky Alfisols with perched water tables, *Clays Clay Miner.*, **45**, 428–439.

## APPENDIX A: DESCRIPTION OF SOIL PROFILES

*Epicalcic Mollic Vertisol (profile 'VR')*

0–25 cm—Humic (Ak1) horizon, tarry black, heavy sandy-clayey, carbonates, vegetation roots;

25–50 cm—Humic (Ak2) horizon, sandy-clayey, slickensides present;

50–88 cm—humic-illuvial horizon (ABk), brown-black, clayey, dense, slickensides present, carbonate concretions and orange-yellow spots;

88–130 cm—Ckg horizon, yellow-brown, carbonate concretions present

Parent rock: Pliocene clays, carbonate-rich.

MAT = 12.5 °C; MAP = 543 mm

*Mollic Vertisol (profile 'JAS')*

0–6 cm—humic—(A1) horizon, dark grey, sandy-clayey, no carbonates

6–40 cm—humic (A2) horizon, black-grey, heavy clayey, dense, slickensides present;

40–100 cm—humic (A3) horizon, tarry black, no carbonates, heavy clayey, slickensides present;

100–140 cm—Transitional AB horizon, dark brown, dense, carbonate and Fe-Mn concretions

140–155 cm—illuvial (Bk) horizon, grey-brown, clayey, carbonate concretions, Fe-Mn concretions present;

155–183 cm—transitional (BCk) horizon, light brown, carbonates and carbonate concretions present;

183–240 cm—Ck horizon, light brown-beige, sandy.

Parent rock: Pliocene clays

MAT = 12.9 °C; MAP = 576 mm

*Stagnic Endogleyic Vertisol (profile SM)*

0–20 cm—humic (A) horizon, light beige-brown, bleached, sandy

20–40 cm—Ag horizon, dark brown-black, sandy-clayey, Fe-Mn concretions and slickensides present;

40–83 cm—illuvial (Btg) horizon, no carbonates, clayey, Fe-Mn concretions and slickensides present;

83–116 cm—BCkg horizon, light beige, carbonate, abundant Fe-Mn concretions, carbonate concretions, small yellow-orange redox spots;

116–140 cm—Ckg horizon, beige, carbonates, abundant yellow-orange redox spots; Fe-Mn concretions present;

Parent material: alluvial-delluvial deposits.

MAT = 12.6 °C; MAP = 768 mm

## APPENDIX B

Content of main and trace elements in selected samples [numbers in column 1 correspond to depth (in cm)] from profiles of Vertisols, obtained from XRF analysis using spectrometer Spectro-X-Lab 2000. For each element the error with one sigma confidence interval is shown in parentheses.

Element dimension	Na %	Mg %	Al %	Si %	P %	S µg/g	Cl µg/g	K %
Profile VR								
2	0.153 (0.054)	0.891 (0.021)	5.852 (0.019)	18.65 (0.03)	0.05936 (0.00093)	823.6 (6)	65.1 (1.1)	1.906 (0.004)
50	<0.15	1.03 (0.024)	6.837 (0.022)	20.34 (0.03)	0.02504 (0.00065)	109.3 (1.8)	23.7 (0.6)	1.792 (0.004)
118	0.211 (0.07)	0.95 (0.024)	6.131 (0.021)	18.76 (0.03)	0.02968 (0.00086)	49 (1.1)	67.9 (1.2)	1.954 (0.005)
Profile JAS								
3	0.208 (0.059)	0.75 (0.021)	6.062 (0.02)	22.48 (0.03)	0.06437 (0.00099)	737.7 (6)	74 (1.2)	1.276 (0.003)
9	0.181 (0.057)	0.771 (0.022)	6.394 (0.021)	23.76 (0.03)	0.04116 (0.00083)	382.3 (4.2)	51.6 (1)	1.239 (0.003)
12	0.217 (0.062)	0.824 (0.022)	6.489 (0.021)	23.92 (0.04)	0.03737 (0.00081)	368.1 (4.1)	205.8 (2.2)	1.228 (0.003)
42	<0.14	0.805 (0.021)	6.63 (0.021)	22.21 (0.03)	0.02073 (0.00058)	94.6 (1.6)	13.4 (0.4)	1.12 (0.003)
66	<0.14	0.855 (0.022)	6.675 (0.021)	22.76 (0.03)	0.01948 (0.00056)	93.4 (1.6)	<2.1	1.124 (0.003)
102	0.218 (0.061)	0.935 (0.022)	6.677 (0.021)	22.46 (0.03)	0.01227 (0.0005)	40.8 (0.8)	9 (0.2)	1.119 (0.003)
132	0.358 (0.072)	1.108 (0.024)	6.953 (0.022)	23.83 (0.04)	0.0148 (0.00056)	69.9 (1.3)	6.1 (0.2)	1.167 (0.003)
144	0.268 (0.069)	0.998 (0.023)	6.129 (0.02)	21.55 (0.03)	0.01399 (0.00066)	149.2 (2.4)	<2.4	1.061 (0.003)
156	0.248 (0.068)	1.051 (0.023)	6.02 (0.02)	21.17 (0.03)	0.02142 (0.00076)	323.4 (3.8)	18.5 (0.6)	1.072 (0.003)
174	0.317 (0.073)	0.954 (0.023)	6.067 (0.02)	21.51 (0.03)	0.01232 (0.00066)	537.1 (5.2)	70.9 (1.3)	1.113 (0.003)
186	0.264 (0.073)	0.828 (0.022)	5.289 (0.019)	18.68 (0.03)	0.01921 (0.00094)	2236 (11)	118.7 (1.7)	1.027 (0.004)
204	0.279 (0.068)	1.003 (0.023)	6.744 (0.021)	23.9 (0.04)	0.02735 (0.0007)	348.8 (4)	133.2 (1.7)	1.486 (0.004)
Profile SM								
2	0.904 (0.08)	0.366 (0.017)	5.413 (0.019)	27.42 (0.04)	0.06477 (0.00098)	616.5 (5.3)	105.8 (1.5)	2.236 (0.004)
10	1.001 (0.085)	0.333 (0.017)	5.846 (0.02)	29.36 (0.04)	0.03713 (0.00076)	223 (3.1)	44.4 (0.9)	2.313 (0.005)
26	0.48 (0.075)	0.663 (0.021)	7.65 (0.023)	24.37 (0.04)	0.01901 (0.00053)	30.5 (0.6)	31 (0.7)	1.756 (0.004)
42	0.413 (0.074)	0.725 (0.022)	7.775 (0.023)	24.61 (0.04)	0.01589 (0.00051)	<20	87.5 (1.4)	1.749 (0.004)
62	0.455 (0.076)	0.76 (0.022)	7.428 (0.022)	24.59 (0.04)	0.02011 (0.00058)	148.1 (2.2)	48.3 (1)	1.847 (0.004)
70	0.504 (0.077)	0.808 (0.022)	7.247 (0.022)	24.64 (0.04)	0.02074 (0.00059)	111.4 (1.8)	90.8 (1.4)	1.906 (0.004)
82	0.401 (0.079)	0.619 (0.021)	5.707 (0.019)	20.25 (0.03)	0.01177 (0.00069)	395 (4.4)	80.5 (1.4)	1.712 (0.005)
94	0.662 (0.09)	0.544 (0.021)	5.202 (0.018)	17.72 (0.03)	0.01078 (0.00078)	1210 (8)	131.9 (1.9)	1.693 (0.005)
134	0.946 (0.087)	0.4 (0.018)	6.697 (0.021)	24.98 (0.04)	0.02306 (0.00072)	83.8 (1.6)	66.3 (1.2)	2.921 (0.006)

(Continued).

Element dimension	Ca %	Ti %	Mn %	Fe %	Zr $\mu\text{g/g}$	Ba $\mu\text{g/g}$	La $\mu\text{g/g}$	Ce $\mu\text{g/g}$
Profile VR								
2	1.748 (0.003)	0.3717 (0.001)	0.0525 (0.00019)	4.557 (0.006)	143.1 (0.7)	417.7 (2)	19.4 (1.9)	50.9 (2.7)
50	1.302 (0.003)	0.4277 (0.001)	0.0478 (0.00018)	5.26 (0.007)	147.9 (0.7)	469.5 (2)	26 (1.9)	63.5 (2.7)
118	5.645 (0.008)	0.355 (0.0011)	0.03269 (0.00018)	5.539 (0.008)	113.3 (0.8)	446.8 (2)	17.6 (1.9)	48.2 (2.7)
Profile JAS								
3	1.487 (0.003)	0.4373 (0.0011)	0.09322 (0.00026)	3.56 (0.006)	278.7 (0.8)	508.3 (2)	37.5 (2)	93.8 (2.7)
9	1.397 (0.003)	0.4661 (0.0011)	0.09526 (0.00026)	3.711 (0.006)	284.9 (0.8)	533.3 (2.1)	36.2 (2)	90.9 (2.7)
12	1.331 (0.003)	0.4718 (0.0011)	0.1005 (0.0003)	3.81 (0.006)	292.2 (0.9)	554.8 (2.1)	40.7 (2)	95.8 (2.7)
42	1.151 (0.003)	0.4635 (0.0011)	0.116 (0.0003)	4.026 (0.006)	285.2 (0.8)	591.4 (2.2)	43.3 (2)	102 (2.8)
66	1.095 (0.002)	0.4758 (0.0011)	0.09691 (0.00026)	3.974 (0.006)	299.9 (0.9)	558.7 (2.1)	43.2 (2)	104.9 (2.8)
102	0.9803 (0.0023)	0.4715 (0.0011)	0.09459 (0.00025)	4.06 (0.006)	280 (0.9)	552 (2.1)	36.9 (2)	93.4 (2.7)
132	1.39 (0.003)	0.4886 (0.0012)	0.09795 (0.00027)	4.11 (0.006)	289 (0.9)	519 (2.1)	38 (2)	92.8 (2.8)
144	5.587 (0.008)	0.4395 (0.0013)	0.09225 (0.0003)	3.691 (0.006)	259.1 (0.9)	373 (1.9)	32.5 (2)	86.1 (2.7)
156	5.949 (0.008)	0.4298 (0.0013)	0.0846 (0.0003)	3.625 (0.006)	248.4 (0.9)	791.9 (2.4)	30.3 (2)	81.4 (2.7)
174	5.78 (0.008)	0.4097 (0.0013)	0.07808 (0.00028)	3.543 (0.006)	233.6 (0.9)	1103 (3)	31.5 (2)	72.6 (2.8)
186	9.863 (0.012)	0.3483 (0.0014)	0.06572 (0.0003)	3.129 (0.006)	189.7 (0.8)	926.5 (2.6)	37.5 (2)	61.5 (2.7)
204	1.33 (0.003)	0.4526 (0.0011)	0.07815 (0.00023)	3.757 (0.006)	258.2 (0.8)	535.4 (2.1)	34.1 (2)	87.4 (2.7)
Profile SM								
2	0.7622 (0.0022)	0.3497 (0.001)	0.09164 (0.00025)	1.77 (0.004)	329.9 (0.9)	936.6 (2.5)	37.1 (1.9)	76.7 (2.6)
10	0.6999 (0.0022)	0.3711 (0.0011)	0.09697 (0.00027)	1.915 (0.004)	360.8 (0.9)	1044 (3)	38 (2)	87.2 (2.7)
26	0.7347 (0.0021)	0.3504 (0.001)	0.06454 (0.0002)	3.646 (0.006)	248.3 (0.8)	850.8 (2.4)	27.9 (1.9)	75.4 (2.7)
42	0.7863 (0.0022)	0.3579 (0.001)	0.08734 (0.00024)	3.826 (0.006)	249.9 (0.8)	852.4 (2.4)	34.9 (2)	91.4 (2.7)
62	0.9511 (0.0025)	0.3485 (0.0011)	0.1372 (0.0003)	3.592 (0.006)	258.5 (0.8)	1445 (3)	56 (2.1)	128 (2.9)
70	1.013 (0.003)	0.3458 (0.001)	0.1356 (0.0003)	3.443 (0.006)	248.8 (0.8)	1088 (3)	51.7 (2)	102 (2.8)
82	9.256 (0.012)	0.2441 (0.0013)	0.2331 (0.0006)	2.676 (0.005)	221 (0.8)	1193 (3)	31.4 (2)	95.6 (2.8)
94	12.72 (0.02)	0.2014 (0.0013)	0.1944 (0.0006)	2.345 (0.005)	185.6 (0.8)	1333 (3)	26.3 (2)	79.7 (2.8)
134	4.988 (0.007)	0.2139 (0.001)	0.02612 (0.00016)	1.929 (0.004)	264.6 (0.9)	1139 (3)	31.8 (1.9)	57.2 (2.7)

APPENDIX C

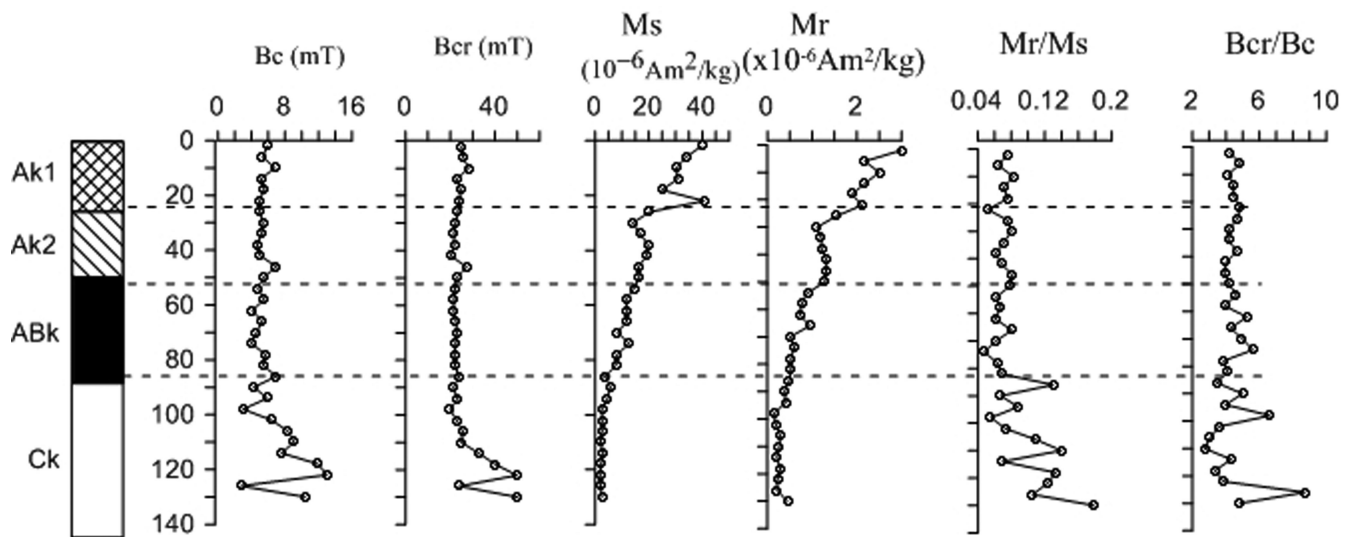


Figure C1. (A) Hysteresis parameters [coercive force (Bc), coercivity of remanence (Bcr), saturation magnetization (Ms), remanent saturation magnetization (Mr)] and ratios Bcr/Bc and Mr/Ms for profile VR.

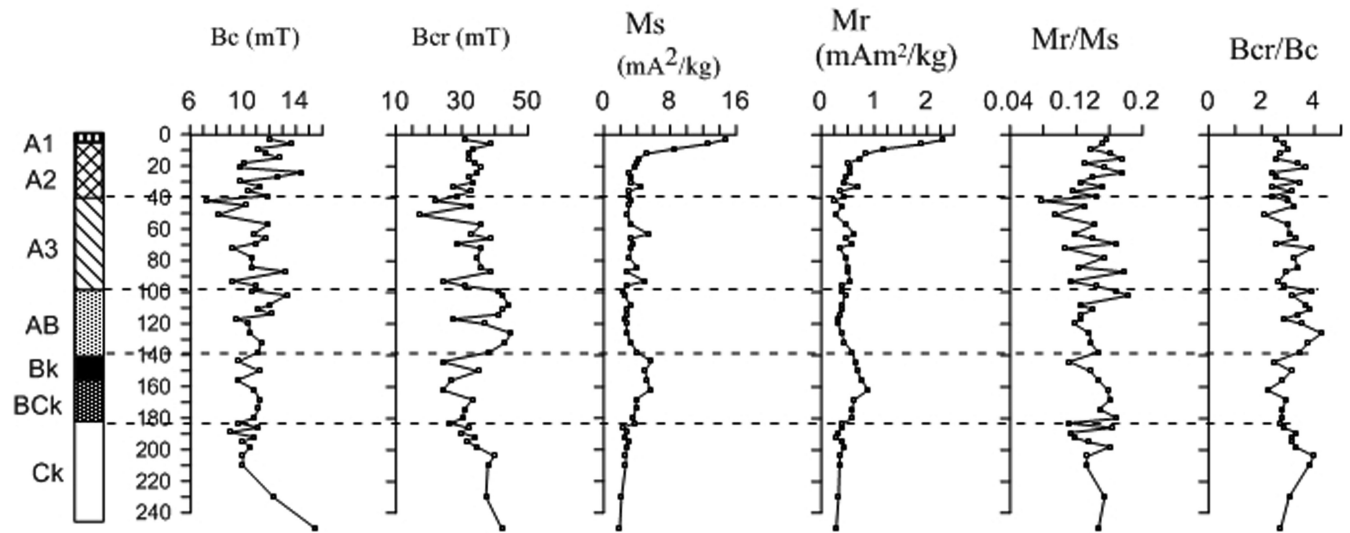


Figure C2. (B) Hysteresis parameters and ratios for profile JAS.

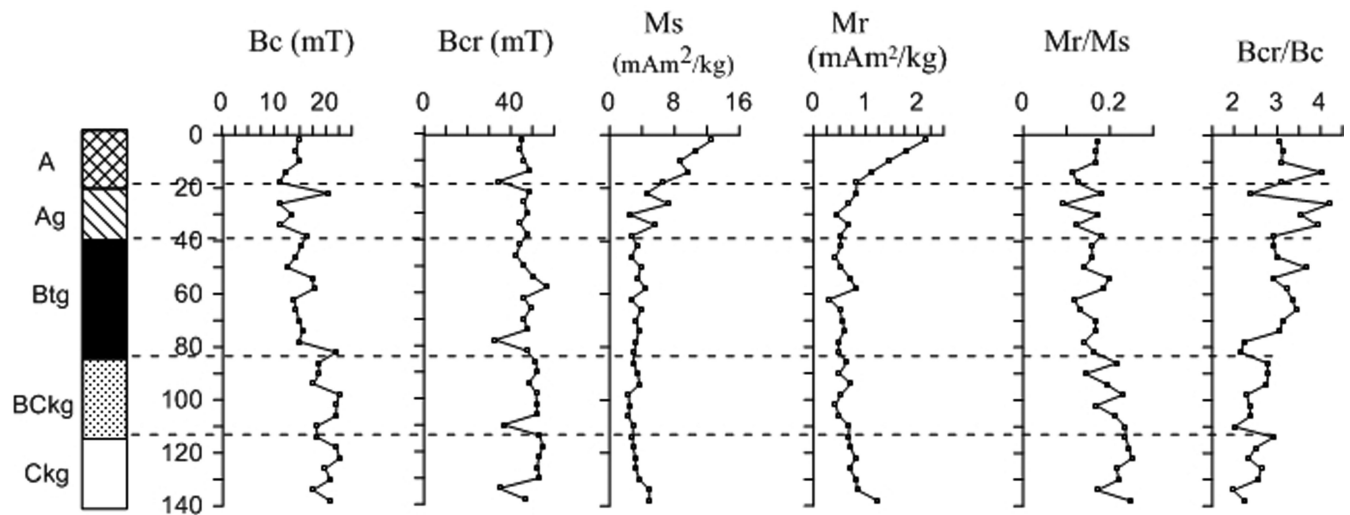


Figure C3. (C) Hysteresis parameters and ratios for profile SM.